Drift og vedlikehold
Fagressurs Drift og vedlikehold
Geofag Drift og vedlikehold 2
29.10.2024

Statens vegvesen

Quality of photogrammetry and LiDAR from UAS

Comparisons of processing workflows, sensors and repeatability assessment

STATENS VEGVESENS RAPPORTER Nr. 1011

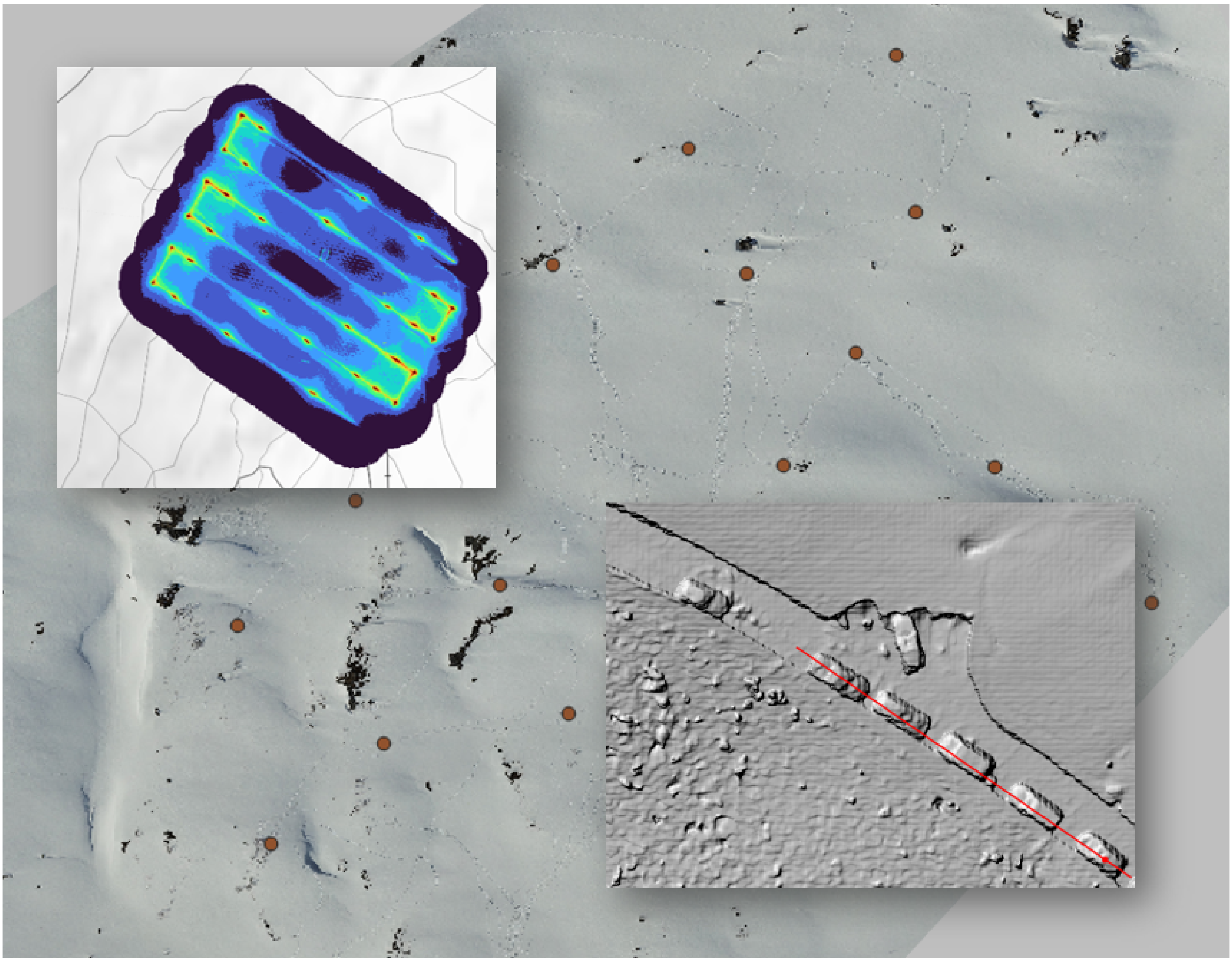

Illustration: GEOSFAIR project

Statens vegvesens rapporter

Tittel
Quality of photogrammetry and LiDAR from UAS

Undertittel
Comparisons of processing workflows, sensors and repeatability assessment

Forfatter
Andrew Tobiesen (editor) with co-authors from SINTEF, NGI and NPRA (see page 3)

Avdeling
Fagressurs Drift og vedlikehold

Seksjon
Geofag Drift og vedlikehold 2

Prosjektnummer
C15115

Rapportnummer
1011

Prosjektleder
Tore Humstad

Godkjent av
Viggo Aronsen

Emneord
UAS, droner, fjernmåling, snø, snøoverflate, snødybde, snøhøyde, snøskred, snøskredvarsling, LiDAR, fotogrammetri

Sammendrag
Rapporten sammenligner repeterbarhet og nøyaktighet av optiske og laserbaserte data som er samlet inn ved hjelp av sensorer montert på droner. Vi undersøker effekten av forskjellige parametere i LiDAR-skanning, som flyhøyde, flyhastighet, skannemønster og sideoverlapp. Rapporten sammenligner også ulike programvarepakker for fotogrammetriprosessering. Funnene viser at både fotogrammetri og LiDAR-undersøkelser kan gi nøyaktige høydemodeller og ortomosaikk når de utføres med avanserte dronesystemer og tilgjengelig programvare. Videre undersøker rapporten repeterbarheten av droneundersøkelser ved å bruke ulike droneplattformer og kamerasystemer.

Antall sider 60

NPRA reports
Norwegian Public Roads Administration

Title
Quality of photogrammetry and LiDAR from UAS

Subtitle
Comparisons of processing workflows, sensors and repeatability assessment

Author
Andrew Tobiesen (editor) with co-authors from SINTEF, NGI and NPRA (see page 3)

Department
O&M Planning and Engineering Services

Section
O&M Geomechanics

Project number
C15115

Report number
1011

Project manager
Tore Humstad

Approved by
Viggo Aronsen

Key words
UAS, remote sensing, snow surface, snow height, avalanche forecasting, LiDAR, photogrammetry

Summary
This report summarizes comparative studies of repeatability and accuracy of optical and laser data recorded with UAS mounted sensors. For photogrammetry surveys, different sensors, different processing software has been used.

The overall conclusions and findings of this work are that both photogrammetry and lidar surveys may give accurate elevation models and orthomosaic using high-end survey drones with current available processing software. We conclude that with this type of technology will be useful and valuable as a part of an integrated workflow for avalanche forecasting.

Pages 60

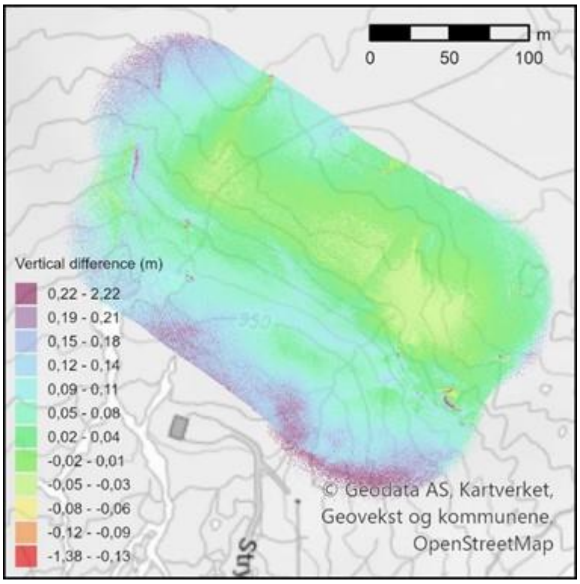

Report

GEOSFAIR (Geohazard survey from the air) deliverable D2.2

Quality assessment of photogrammetry and LiDAR measurements: comparisons of processing workflows, sensors and repeatability assessment

Authors:

Andrew Tobiesen, Elisabeth Hoffstad Reutz, Sean Salazar, Bastien Dupuy, Halgeir Dahle, Arnt Grøver, Regula Frauenfelder, Emil Solbakken, Tore Humstad, Edward McCormack

Report No: 2024:01233

Clients and partners:

The research council of Norway, NPRA, NGI

SINTEF Industry
Postal address:
Postboks 4763 Torgarden
7465 Trondheim

Switchboard: +47 40005100

info@sintef.no

Enterprise /VAT No:
NO 919 303 808 MVA

Report

GEOSFAIR (Geohazard survey from the air) deliverable D2.2

Quality assessment of photogrammetry and LiDAR measurements: comparisons of processing workflows, sensors and repeatability assessment

KEYWORDS
UAS, remote sensing, snow surface, snow height, avalanche forecasting, LiDAR, photogrammetry

VERSION
4

DATE
2024-10-29

AUTHORS
Andrew Tobiesen, Elisabeth Hoffstad Reutz, Sean Salazar, Bastien Dupuy, Halgeir Dahle, Arnt Grøver, Regula Frauenfelder, Emil Solbakken, Tore Humstad, Edward McCormack

CLIENT AND PARTNERS
The research council of Norway, NPRA, NGI

CLIENT'S REFERENCE
321035/080

PROJECT NO.
102025034

NO. OF PAGES
57

SUMMARY
This report summarizes comparative studies of repeatability and accuracy of optical and laser data recorded with UAS mounted sensors. For photogrammetry surveys, different sensors, different processing software has been used. The overall conclusions and findings of this work are that both photogrammetry and lidar surveys may give accurate elevation models and orthomodels using high-end survey drones with current available processing software. We conclude that with this type of technology will be useful and valuable as a part of an integrated workflow for avalanche forecasting.

PREPARED BY Bastien Dupuy	SIGNATURE
CHECKED BY Madeline Lee	SIGNATURE
APPROVED BY Peder Eliasson	SIGNATURE

REPORT NO.	ISBN	CLASSIFICATION	CLASSIFICATION THIS PAGE
2024:01233	978-82-14-07114-6	Unrestricted	Unrestricted

Document history

VERSION	DATE	VERSION DESCRIPTION
1	2023-05-26	Initial version gathering photogrammetry tests
2	2023-09-02	LiDAR tests are added
3	2024-08-19	Consistency updates, clean version ready for proofreading
4	2024-10-29	Final version

Table of contents

1. Executive summary 5

2. LiDAR part 8

2.1 Motivation 8

2.2 Method 8

2.3 Repeatability 10

2.3.1 Point density 10

2.4 Influence of flight height 11

2.4.1 Point density 11

2.4.2 Profiles 12

2.5 Influence of flight speed 15

2.5.1 Point density 15

2.5.2 Profiles 15

2.6 Influence of scanning patterns 17

2.6.1 Point density 17

2.6.2 Profiles 17

2.7 Influence of different LiDAR side overlap 18

2.7.1 Point density 19

2.7.2 Profiles 19

2.8 Vertical variability 21

2.9 Influence of equipment and flight height 22

2.10 Comparison of LiDAR-derived snow height to snow height measurements with a snow probe .23

3. Photogrammetry part 26

3.1 Motivation 26

3.2 Summary and observations 26

3.2.1 Mod_ODM 26

3.2.2 Metashape 27

3.2.3 Sitescan 27

3.2.4 Datact 28

3.3 Reference model 28

3.3.1 Ground truth and ground control points 28

3.3.2 Reference model for the M300_Breiddalen#1 dataset 29

3.4 Comparison of different processing software using the Breiddalen#1 M300 dataset 34

3.4.1 Visual comparisons of orthophotos 34

3.4.2 Terrain profile comparisons for the 4 software packages 36

3.4.3 Hillshade slice comparisons 38

3.4.4 Cars and depth resolution 41

3.5 Comparison using the Breiddalen#2 Phantom 4 dataset 46

3.5.1 Visual comparison 46

3.5.2 Elevation transects using the Breidallen#2 Phantom 4 dataset 49

3.6 Comparison of different UAS platform and camera payloads 53

3.6.1 Repeatability of surveys 53

Appendix 1 55

Preprocessing and Image Optimization for Snowy Terrain 55

Image Preprocessing after Acquisition 55

APPENDICES

Klikk eller trykk her for å skrive inn tekst.

List of abbreviations:

DEM: digital elevation model
GCP: ground control point
GPS: global positioning system
GNSS: global navigation satellite system
LiDAR: light detection and ranging
RGB: red green blue
RTK: real-time kinematics
SfM: structure from motion
UAS: uncrewed aerial system
AGL: above ground level

1. Executive summary

This report summarizes comparative studies of repeatability and accuracy of optical and laser data recorded with UAS mounted sensors. For photogrammetry surveys, different sensors, different processing software has been used. The Lidar survey part is prepared by NGI and described in the first part of the report and is using dataset recorded at Fonnbu NGI avalanche research station in Strynefjellet.

The photogrammetry part is prepared by SINTEF using datasets obtained from several locations including datasets from Breiddalen. The image sets were gathered by NGI and NPRA using DJI drones (Matrice 300 RTK and Phantom Pro 4 RTK). Photogrammetry processing using commercial software was conducted by NGI and NPRA.

The overall conclusions and findings of this work are that both photogrammetry and lidar surveys may give accurate elevation models and orthomodels using high-end survey drones with current available processing software. These models can then be used as basis for further evaluation of exposed areas such snow layer analysis for estimation of avalanche dangers. As these drones can be operated semi or fully automatic, it is, with well-established software tools, possible to create efficient workflows such that the method of creating these types of valuable results can be done automatically, repeatable and in a reasonably short timeframe. We conclude that this type of technology will be useful and valuable as a part of an integrated workflow for avalanche forecasting.

For the photogrammetry part, we have made comparisons with different available software packages for elevation model creation. We found that some packages work better than others, however, this may be due to sub-optimal software parameter tuning for creating the different models and may not necessarily be due to worse software performance. The results are also produced to show visual differences and evaluated based on our assumed optimal software settings and available compute resources. Limited statistical analysis of the overall performance has been done, as the main effort was done programming workflows. An interesting point to note is that preprocessing of images over large areas of snow, using adaptive histogram algorithms to enhance details, significantly improved the final elevation models when using the open-source pathway. We included this as an automated part of the preprocessing of images workflow.

Findings LiDAR:

This lidar study has looked at the effect of changing various parameters in UAS-based LiDAR scanning surveys carried out to capture snow surface height and snow surface characteristics. The findings from our tests are summarized below:

- The repeatability between two surveys taken at different points in time (within 1 hour) is good. The average point density is almost the same, and the distribution of how the point density varies throughout the survey pattern is similar.
- As expected, increasing flight altitude considerably reduces point density. The vertical variability between the flights at 60 m and 80 m altitude overlaps, while the flight with 100 m altitude differs from the first two with about 0.1 m.
- Also, increasing flight speed reduces point density, as expected. There is some variability in the recorded surface height, but this might be due to a change in the snow coverage between the flights.
- The use of a non-repetitive versus a repetitive scan pattern affects the average point density only to a small degree, with the point density being slightly higher for the repetitive survey. However, the largest difference between the two scan modes is the pattern of the distributed point density which clearly differs.
- Higher LiDAR side overlap yields a higher point density but requires a larger number of transects to cover the survey area.
- Choosing five ground control points and comparing their measured height in each independent flight shows that the vertical variability between surveys collected during the same time period is less than 0.1 m.
- In general, the different surveys record similar snow surfaces. However, the accurate capture of the 3D-generation of steep edges and sections with large height differences - as found at the edge of the roof of the research station – varies between different surveys.
- Through this study, the need to collect an additional higher resolution bare earth model has been revealed. This to be able to consistently work in the same resolution of the captured lidar data. Currently, the available bare earth reference model has a maximum resolution of 0.5 m, in which small details might not appear.
- Due to the limited data used in this Lidar, there is a need to create more snow probe measurements with georeferenced points, to make a statistical analysis of how good the LiDAR-based snow height maps are, and its use for rapid snow surface mapping.

Findings Photogrammetry:

- Real-Time Kinematic Global Positioning System (RTK) can be used for georeferencing elevation models, down to decimeter/centimeter precision, but the quality varies depending on processing software workflows, drone characteristics and survey execution and finding an optimum set of software parameters.
- A "ground truth" model was tested in comparison with the RTK-generated models with a limited number of ground control points (GCP). It is unclear if the created model has a higher absolute position accuracy compared to the ground truth model.
- Visual observation of the RTK models against GCP's added in post on the orthomodel shows good results for some processing software, but not that good for others.
- Pre-processing of the raw images was helpful to obtain consistent results along a large area of snow, because of varying weather and light conditions. The images are typically under-exposed or have white balance variations. The consequence is loss of details over certain areas of the snowy surfaces,

which again cause pixelation and noise during model creation. A pre-processor plugin has been developed that corrects for this in batch.

- The models from Sitescan software and MOD_ODM software showed consistency along the different datasets, high depth resolution and consistent elevation profiles along transects. The Sitescan DEM's are noisy in areas where there are larger areas of snow. This is similar to the errors found with the MOD_ODM models prior to using the image enhancing technique. The models calculated with the Datact software were erroneous in the georeferencing process (this was found not to be systematic, but more random errors of more than 60 cm across sets). The assumed absolute and relative vertical accuracy is in the range of +/- 10 cm or lower for the best models.
- The produced model using GCP's, i.e., the "reference model", seems to have improved georeferencing relative to the RTK-models. However, the differences are very small (a few centimeters), and for the specific model generated, the 3D-reconstruction errors were slightly larger than the RTK-referenced models. The GCP model did not use the pre-processing of images.

2. LiDAR part

2.1 Motivation

A sensitivity study has been performed to investigate how different parameters in a UAS-based LiDAR survey affect the output results. The sensitivity study has been executed by varying one variable for each flight, to assess how this affects the output results. This to:

- Look at the change in point density between repetitive UAS surveys over snow.
- Compare the difference in point density distribution when varying input parameters to a UAS survey.
- Analyze the difference in recorded surface height between UAS surveys taken within a small time-interval.
- Compare a surface model created from LiDAR data to a surface model created by the interpolation of snow-probe measurements.

2.2 Method

In total nine flights have been carried out to analyze how the changes of various settings affect the point clouds collected by a UAS-mounted LiDAR. The flights have been conducted during winter, and hence record the snow surface height. The varied parameters are flight speed, flight altitude, scanning pattern and LiDAR side overlap. An overview of the parameters that were varied can be found in Table 2.2-1.

The point density, and the point density distribution (given in points per square meter) are analyzed to find out how different parameters affect these outputs. Profiles are also created to investigate if the different parameters affect the recording of the surface. The vertical variability is also investigated. The statistics of the point density have been obtained with the tool "zonal statistics" in QGIS. The point clouds have been cleaned using CloudCompare software and exported both as rasters with a 0.1 m x 0.1 m resolution, and as a 1 m x 1 m resolution raster displaying the number of points cell.

The UAS-based LiDAR surveys have been carried out close to NGI's research station Fonnbu (Strynefjell mountains, Vestland county), displayed in Figure 2.2-1. The survey area is displayed in Figure 2.2-2, with the red square outlining the survey area, and the white square indicating the position of the Fonnbu research station. To calculate the absolute snow depth a 0.5 m x 0.5 m, a digital terrain model from *hoydedata.no* (airborne LiDAR), collected in 2022, was used.

Table 2.2-1: Overview of the parameters that have been changed during the different LiDAR surveys. Cells marked in blue highlight parameters that differ between subsequent flights and the two initial flights (in week 9 and fl1 in week 11).

Survey name	week 9	fl1, week 11	fl2, week 11	fl3, week 11	fl4, week 11	fl5, week 11	fl6, week 11	fl7, week 11	fl8, week 11
Flight altitude	80 m	80 m	100 m	60 m	80 m	80 m	80 m	80 m	80 m
Terrain aware	ASTER	ASTER	ASTER	ASTER	ASTER	ASTER	ASTER	ASTER	ASTER
LiDAR side overlap	50%	50%	50%	50%	50%	50%	50%	35%	20%
Image forward overlap	80%	80%	80%	80%	80%	80%	80%	80%	80%
Timed interval	yes	yes	yes	yes	yes	yes	yes	yes	yes
Margin	10 m	10 m	10 m	10 m	10 m	10 m	10 m	10 m	10 m
Scanning pattern	non-repetitive	non-repetitive	non-repetitive	non-repetitive	non-repetitive	repetitive	non-repetitive	non-repetitive	non-repetitive
Dual return	240 kHz	240 kHz	240 kHz	240 kHz	240 kHz	240 kHz	240 kHz	240 kHz	240 kHz
Speed	4 m/s	4 m/s	4 m/s	4 m/s	6.4 m/s	4 m/s	10 m/s	10 m/s	10 m/s
Course angle	298	298	298	298	298	298	298	298	298
Elevation optimized	yes	yes	yes	yes	yes	yes	yes	yes	yes
Elevation optimized	yes	yes	yes	yes	yes	yes	yes	yes	yes

Figure 2.2-1: Left: Fonnbu research station during summer (Norgeibilder.no, Stryn 2020). Right: Orthomosaic of Fonnbu research station during winter, created from an optical dataset collected in this study.

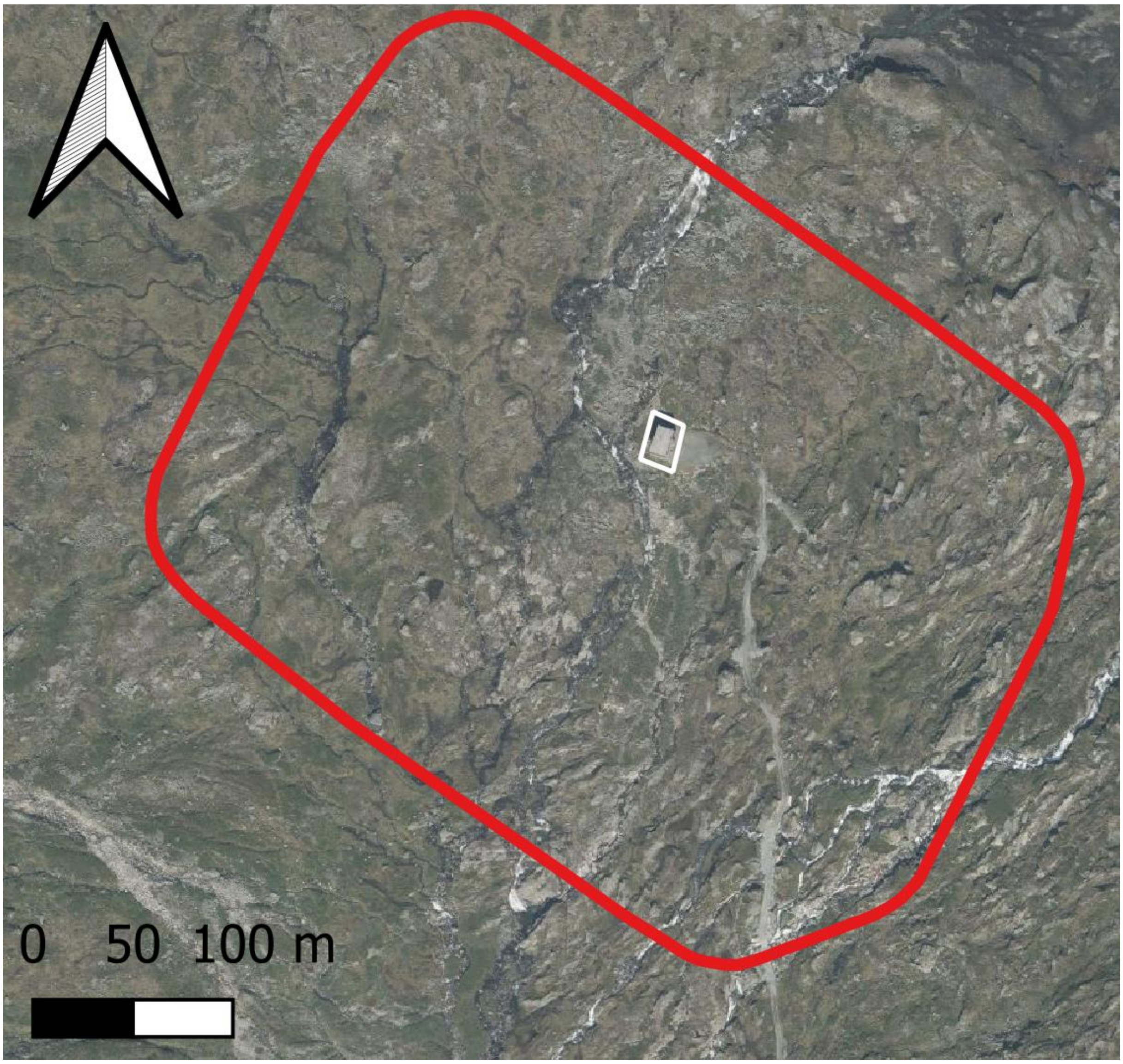

Figure 2.2-2: The red square outlines the study area, the white square gives the position of the Fonnbu research station.

2.3 Repeatability

To analyze how a LiDAR survey with the same parameters can differ between flights, a survey with the same settings was carried out in both week 9 and week 11 (fl1). The flight from week 9 covers a smaller area than the flight from week 11, other than that their flight parameters are identical. The settings used in these surveys can be found in Table 2.2-1.

2.3.1 Point density

Table 2.3.1-1 displays statistics for the point density of the two surveys. Overall, the values are quite similar, with the *week 9* survey having a slightly higher mean value of the point density than *week 11 fl1*. Meteorological factors might be a possible explanation for this, as the *week 11 fl1* scan was carried out during a period with some fog, which probably caused more scattering of the LiDAR signal. The flights show the same overall distribution of the point density (Figure 2.2-1).

Table 2.3.1-1: statistics of points per square meter for surveys of week 9 and fl1 week 11.

Survey	Mean [pts/sqm]	SD [pts/sqm]	Min [pts/sqm]	Max [pts/sqm]
week 9	1039	583	1	5013
week 11 fl1	1001	581	1	5013

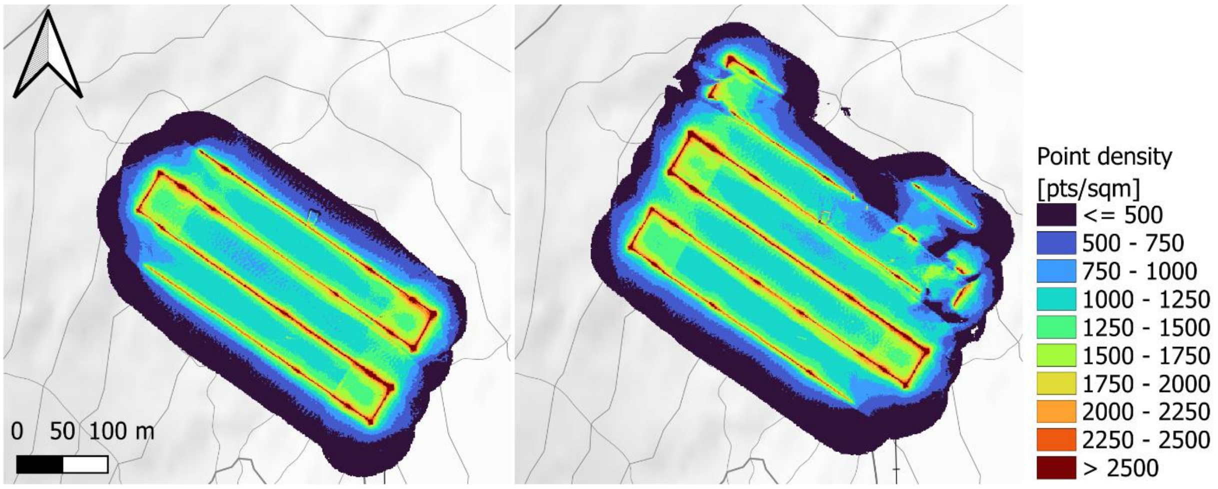

Figure 2.3.1-1: Repeatability test. Distribution of the point density for survey week 9 (left), and survey week 11 fl1 (right).

2.4 Influence of flight height

To evaluate how the flight altitude affects the result of the LiDAR scan, three different flight heights were tested. The settings used in the surveys can be found in Table 2.2-1. Three profiles were created, to analyze how the measured surfaces differ.

2.4.1 Point density

Table 2.4.1-1: statistics of points per square meter for the different surveys carried out to study the effect of flight height on point density and vertical variability: fl1, fl2, fl3, all flown in week 11. Table 2.4.1-1 summarizes the statistics of the point density in each of the three surveys. Figure 2.4.1-1 illustrates that the mean point density is significantly reduced with increasing flight altitude. The maximum point density within a square meter is also reduced. On the other hand, as flight height increases, the number of “laps” needed to cover the entire survey area is reduced.

Table 2.4.1-1: statistics of points per square meter for the different surveys carried out to study the effect of flight height on point density and vertical variability: fl1, fl2, fl3, all flown in week 11.

Survey	Flight altitude	Mean [pts/sqm]	SD [pts/sqm]	Min [pts/sqm]	Max [pts/sqm]
fl3, week 11	60 m AGL	1614	781	1	7981
fl1, week 11	80 m AGL	1001	581	1	5013
fl2, week 11	100 m AGL	791	436	1	3827

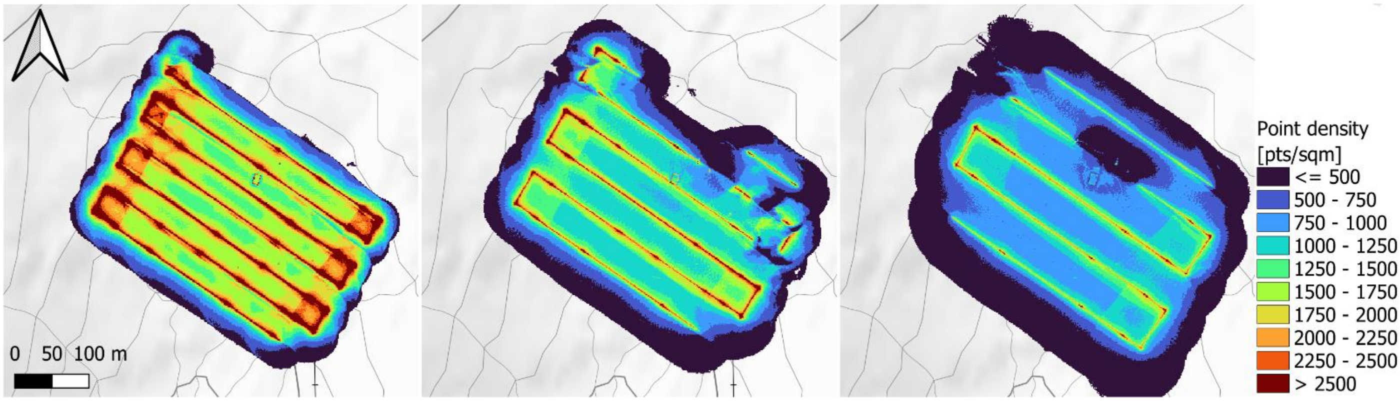

Figure 2.4.1-1: Influence of flight height on point density. From left to right: fl3 (60 m), fl1 (80 m) and fl2 (100 m agl) surveys. The sequence clearly illustrates that point density is increasing with decreasing flight height.

2.4.2 Profiles

Three profiles were taken to specifically analyze the variability between surveys induced by changes in vertical flight height. Figure 2.5 displays the location of the three profiles. Two profiles are captured across the research station to see how well they depict the building edges, and a small, shorter profile is located approximately 13 meters eastwards of the research station. The datasets are collected within a short period (within 1 hour for fl1-fl5, and within 30 minutes for fl6-fl8). Nevertheless, the snow surface might have experienced some small changes (e.g., due to changes in air temperatures, radiation or wind transport during the sensing period) between the collections, which must be accounted for during interpretation.

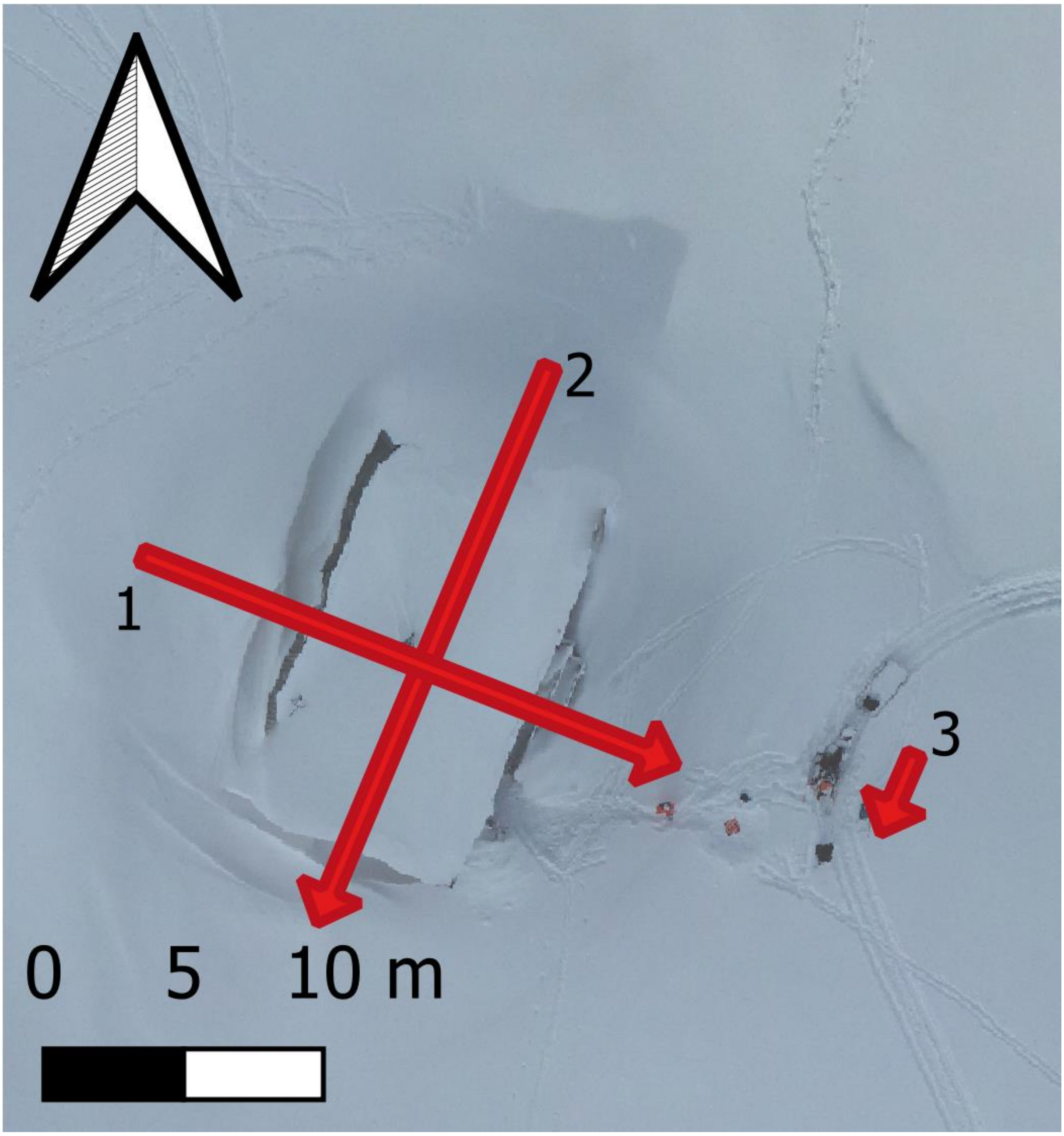

Figure 2.4.2-1: Location of the profiles taken above and in front of Fonnbu research station, with the arrows showing the direction of the profiles. The orthomosaic is the same than Figure 2-1.

From profiles 1 and 2 in Figure 2-6, we observe that the differences between the recorded surfaces over the roof are quite small. Profile 1 of survey fl1 shows some dips/trenches that one would not necessarily expect to observe on a roof. The north-western (1) and northern (2) edge of the research station is perceived similar in all three flights, with the trench between the wind-accumulated snow and the roof of the research station is captured well in all three flights. The south-eastern and southern edges are captured slightly different between the flights, with the biggest deviation between fl1 (60 m) and fl2 (100 m) surveys on the southern edge of the station. Profiles 3 fl3 (60 m) and fl1 (80 m) surveys almost overlap, while fl2 (100 m) survey deviates from the two with approximately 10 cm difference.

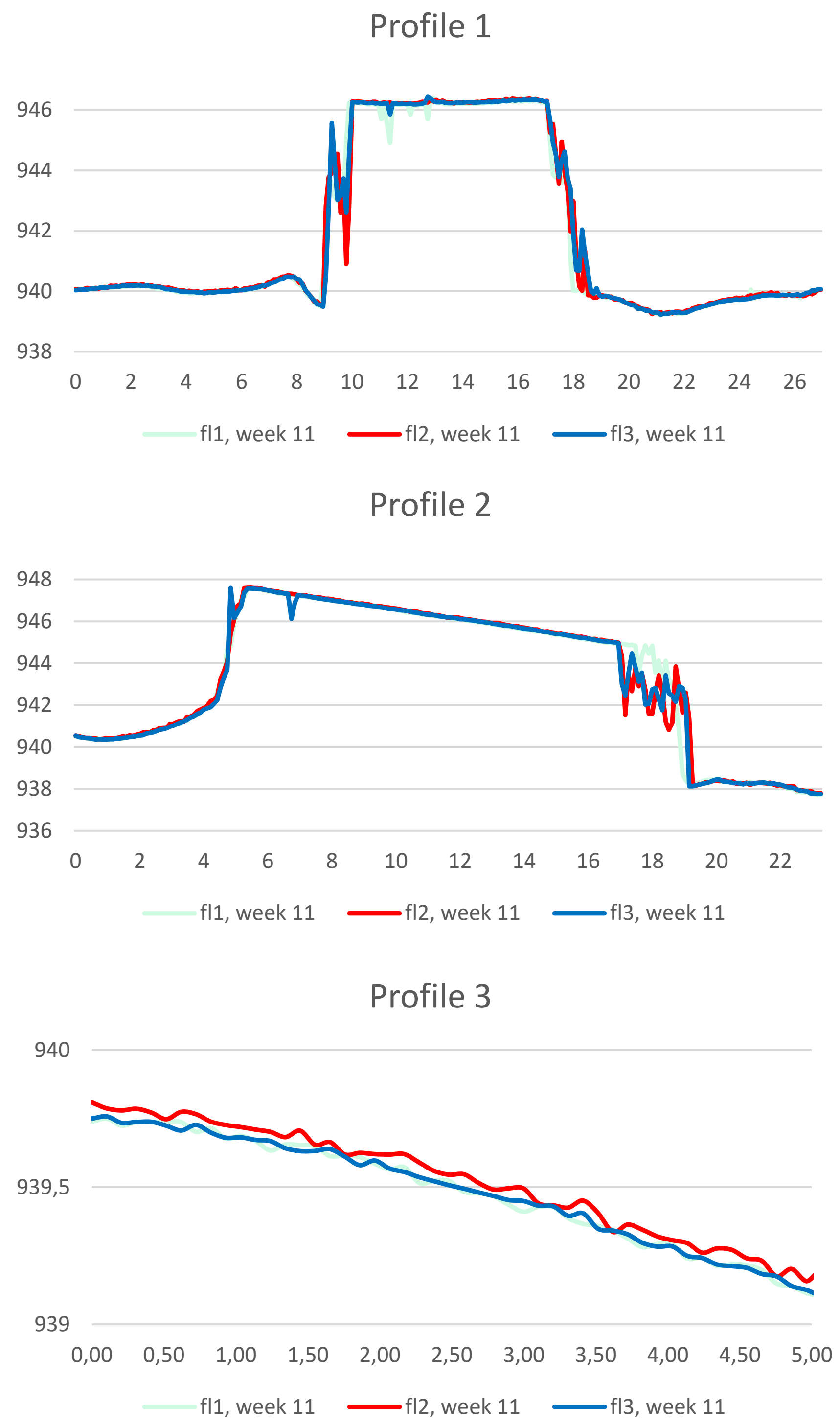

Figure 2.4.2-2: Flight profiles across and in front of Fonnbu research station. fl1 survey (green lines) was flown at 80 m flight height, fl2 survey (red lines) at 100 m and fl3 survey (blue lines) at 60 m. Horizontal and vertical scales are in m.

2.5 Influence of flight speed

Three LiDAR surveys have been flown with different flight speed, to analyze how differences in flight speed affect the output. The survey settings can be found in Table 2.2-1. Three profiles are created to analyze how the results differ between surveys.

2.5.1 Point density

When increasing the flight speed, the mean density and the maximum value are reduced (see Table 2.5.1-1). The reduction is similar when going from 4 to 6.4 m/s, and when increasing from 6.4 to 10 m/s. Figure 2-7 also displays this pattern, i.e., a reduction in point density along the flight path as the flight speed increases. The number of "laps" of the flight path needed to cover the entire survey area remains the same when the flight speed is changed.

Table 2.5.1-1: statistics of points per square meter for the different surveys; fl1, fl4, fl6, week 11, flown with different flight speeds to study effect on point density and vertical variability.

Survey	Flight speed	Mean [pts/sqm]	SD [pts/sqm]	Min [pts/sqm]	Max [pts/sqm]
fl1, week 11	4 m/s	1001	581	1	5013
fl4, week 11	6.4 m/s	823	446	1	4906
fl6, week 11	10 m/s	669	395	1	4802

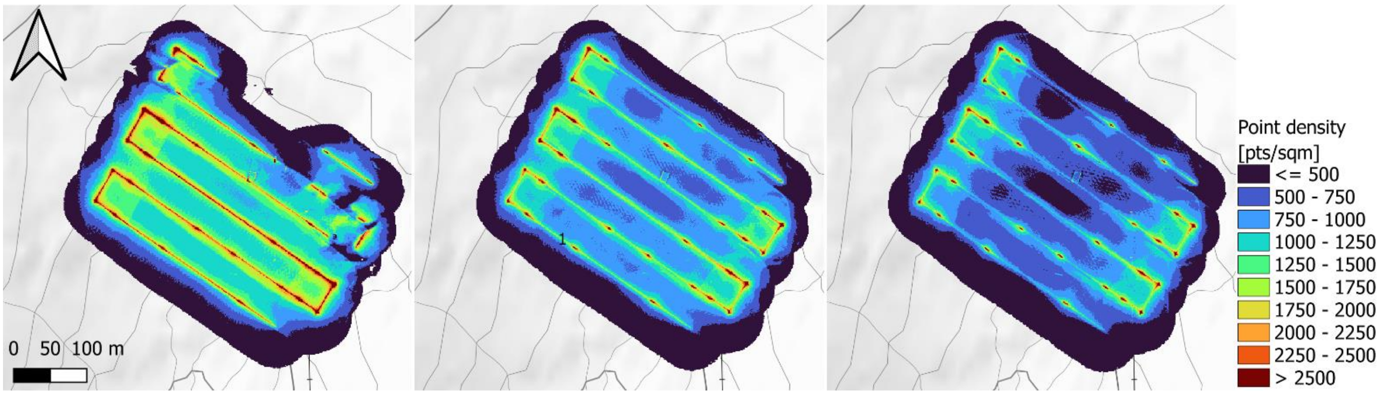

Figure 2.5.1-1: Influence of flight speed on point density. From left to right: fl1 (4 m/s), fl4 (6.4 m/s) and fl6 (10 m/s) surveys. Increasing flight speed leads to a reduction in point density.

2.5.2 Profiles

The same three profiles displayed in Figure 2.4.2-1 are used to analyze if there is a difference in the recorded surface between surveys carried out with different flight speeds. The dataset of fl1 and fl4 surveys are collected quite close in time (within 1 hour), while fl6 survey was collected 6 hours later the same day. From profile 1 and 2 in Figure 2.5.2-1, the roof height seems similar, while the recorded edge of the research station differs. In Profile 1, it seems like all the flights measure some dips which one would not expect to see on a roof. In profile 3, the results of fl1 and fl4 surveys differ with around 0.1 m, while fl6 survey shows another shape than fl1 and fl4 surveys. This new surface shape can probably be explained due to actual changes in the snow cover between the flights and is not related to change in flight speed.

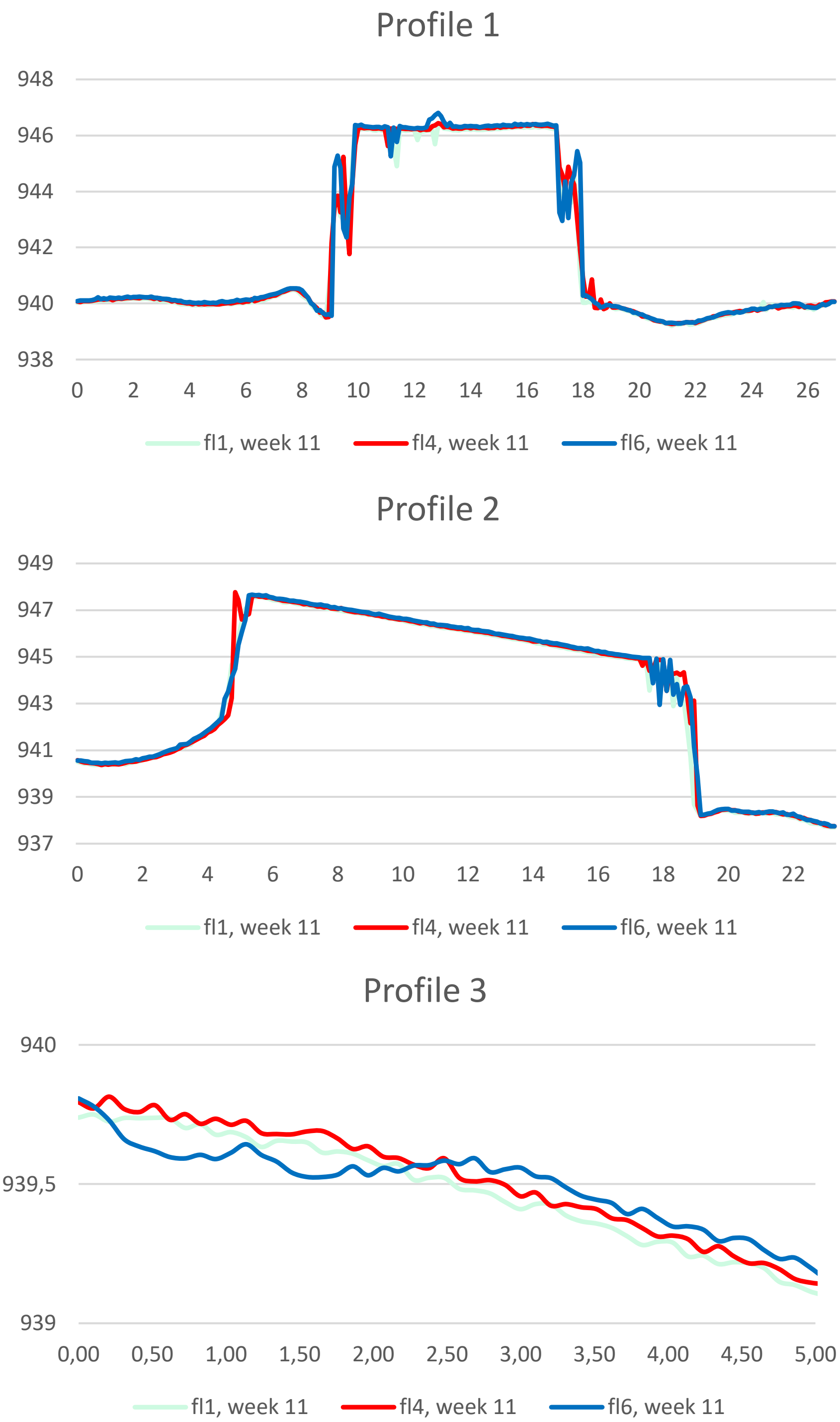

Figure 2.5.2-1: Flight profiles across and in front of Fonnbu research station. fl1 survey (green lines) was flown at 4 m/s flight speed, fl4 survey (red lines) at 6.4 m/s and fl6 survey (blue lines) at 10 m/s. Horizontal and vertical scales are in m.

2.6 Influence of scanning patterns

Two flights were carried out to check how different scanning patterns affect the output. One scan was carried out with the repetitive scanning pattern and one with the non-repetitive scanning pattern. The remaining variables were kept the same and can be found in Table 2.2-1. Three profiles were created to assess how they differ between the surveys.

2.6.1 Point density

The survey using the repetitive scanning pattern shows a higher mean and maximum point density per square meter as compared to the one with the non-repetitive scanning pattern (Table 2**.6.1-1**). Figure 2.6.1-1 displays the point density distribution and shows there is quite a large difference between the two scanning patterns. The non-repetitive survey has a clear flight path that can be seen in the distribution of point density, while this is not as evident for the repetitive survey.

Table 2.6.1-1: statistics of points per square meter for the different surveys; fl1 and fl5, week 11. The LiDAR scanning pattern is varied to study the effect on point cloud.

Survey	Scanning pattern	Mean [pts/sqm]	SD [pts/sqm]	Min [pts/sqm]	Max [pts/sqm]
fl1, week 11	non-repetitive	1001	581	1	5013
fl5, week 11	repetitive	1171	751	1	8585

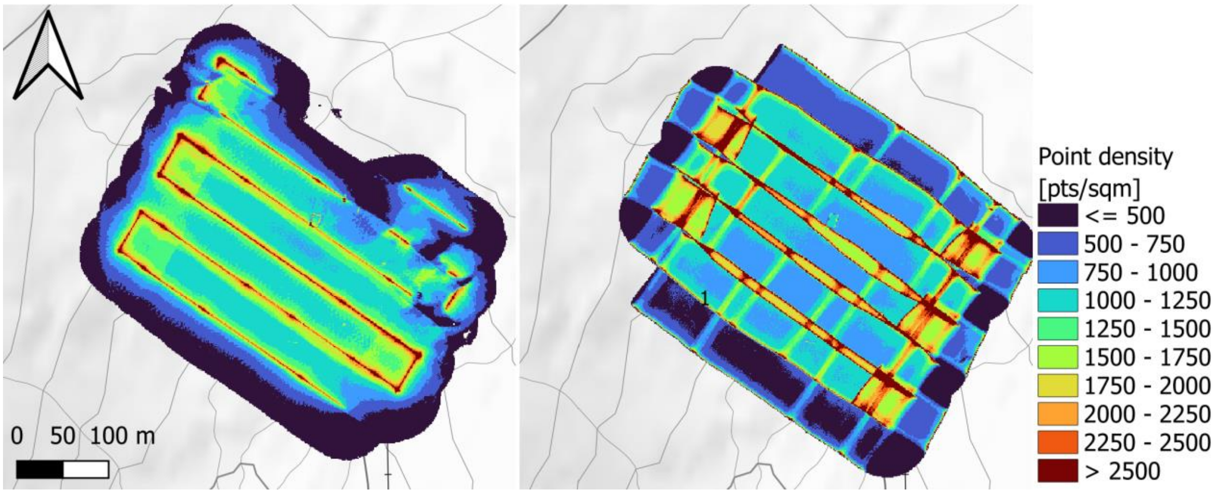

Figure 2.6.1-1: Influence of scanning pattern on point density. From left to right: fl1 (non-repetitive) and fl5 (repetitive) surveys.

2.6.2 Profiles

The same three profiles displayed in Figure 2.4.2-1 are used to analyze if there is a difference in the recorded surface between the two different scanning patterns. The datasets were collected within a short time-period (within 1 hour). From Profile 1 in Figure 2**.6.2-1**, we observe that fl1 survey has dips across the roof, while this is not observed for fl5 survey. The two flights overlap quite good in profile 2, but the capturing of the edge of the research station differs between the two scans. There is a difference of approximately 0.1 m between the two filghts in profile 3. Since this difference is quite even, it is difficult to determine if it is due to a change in the snow surface between scans, or due to differences in the recorded surface.

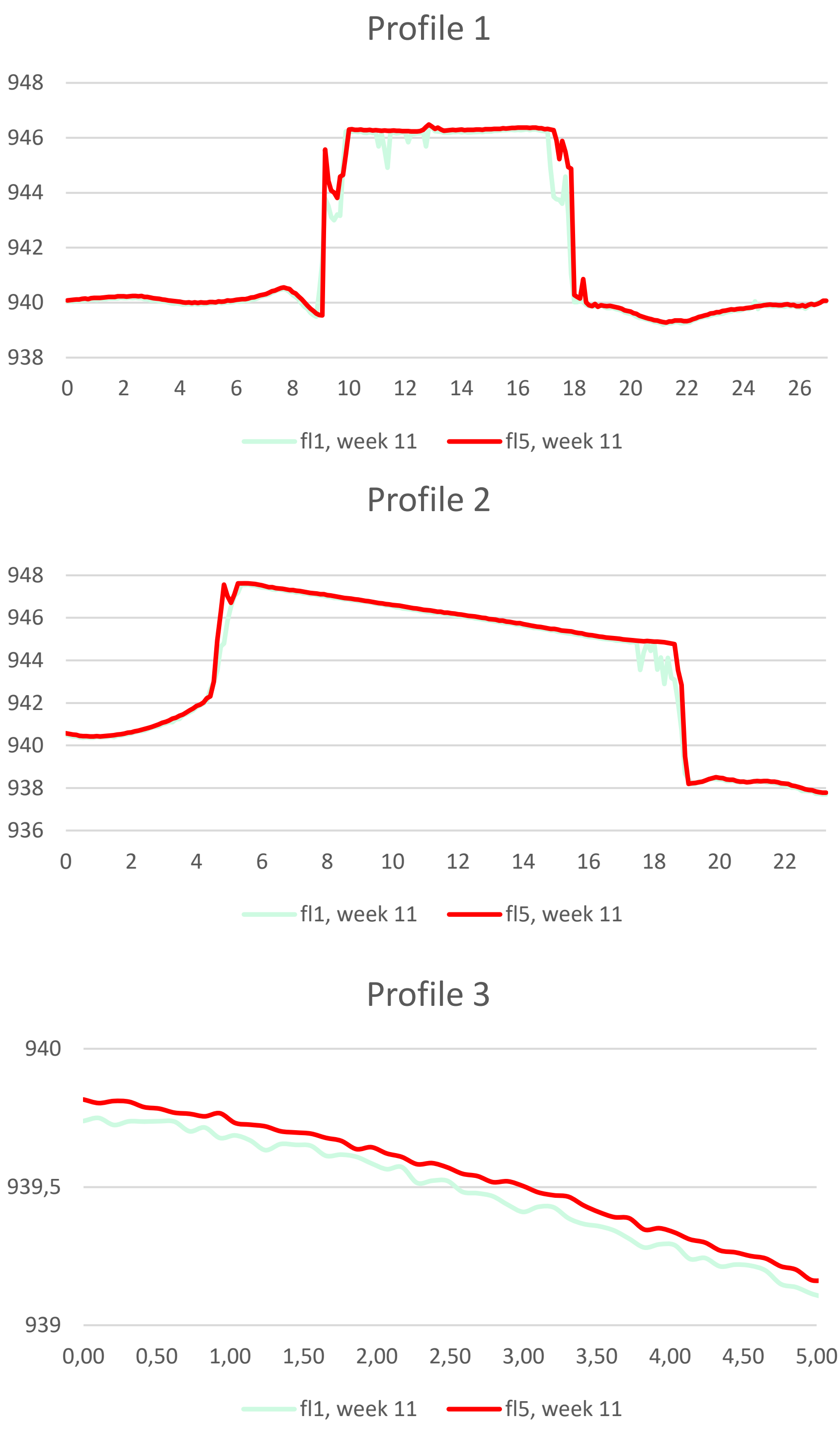

Figure 2.6.2-1: flight profiles across and in front of Fonnbu research station. fl1 survey (green lines) was flown with a non-repetitive scanning pattern and fl5 survey (red lines) with a repetitive scanning pattern. Horizontal and vertical scales are in m.

2.7 Influence of different LiDAR side overlap

Three flights were carried out to check how LiDAR side overlap affects the results. These surveys were taken during night, at 10 m/s flight speed and without the collection of RGB images. An overview of the acquisition parameters can be found in Table 2.2-1. Three profiles were created to assess how they differ between the surveys.

2.7.1 Point density

Higher LiDAR side overlap leads to a higher point density, both for the mean value and the maximum value (Table 2.7.1-1). A higher overlap-percentage requires the UAS flight laps to be quite close to each other. The closeness of the laps decreases with a reduction in overlap, hence the number of laps to cover the survey area also decreases. This causes the point density to be lower for a lower overlap-percentage. The density right under the laps seems quite similar.

Table 2.7.1-1: statistics of points per square meter for the different surveys: fl6, fl7 and fl8 surveys, week 11.

Survey	LiDAR side overlap	RGB	Flight speed	Mean [pts/sqm]	SD [pts/sqm]	Min [pts/sqm]	Max [pts/sqm]
fl6, week 11	50%	no	10 m/s	669	395	1	4802
fl7, week 11	35%	no	10 m/s	554	323	1	4382
fl8, week 11	20%	no	10 m/s	473	301	1	4514

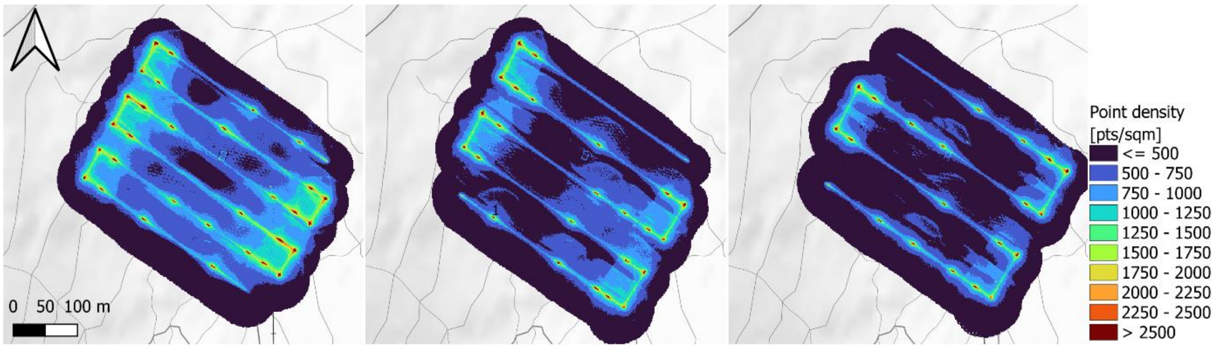

Figure 2.7.1-1: Influence of LiDAR side overlap on point density. From left to right: fl6 (50%), fl7 (35%) and fl8 (20%) surveys.

2.7.2 Profiles

The three profiles displayed in Figure 2.4.2-1 are used to check if there is a difference in the recorded surface with different image overlap. The datasets are collected within a short time period (within 30 minutes). The profiles presented in

Figure 2.7.2-1 displays the same trends as already observed in the other tests. Profile 1 has some flights with peaks and dips over the roof. fl7 survey has a large peak on the middle of the roof while fl6 and fl8 surveys have some dips. The recording of the edge varies. In profile 2, there is a good overlap between the different scans at the roof, but the far side edge is recorded differently between the three scans. All the flights have the same recorded surface shape, and they differ with around 0.1 m.

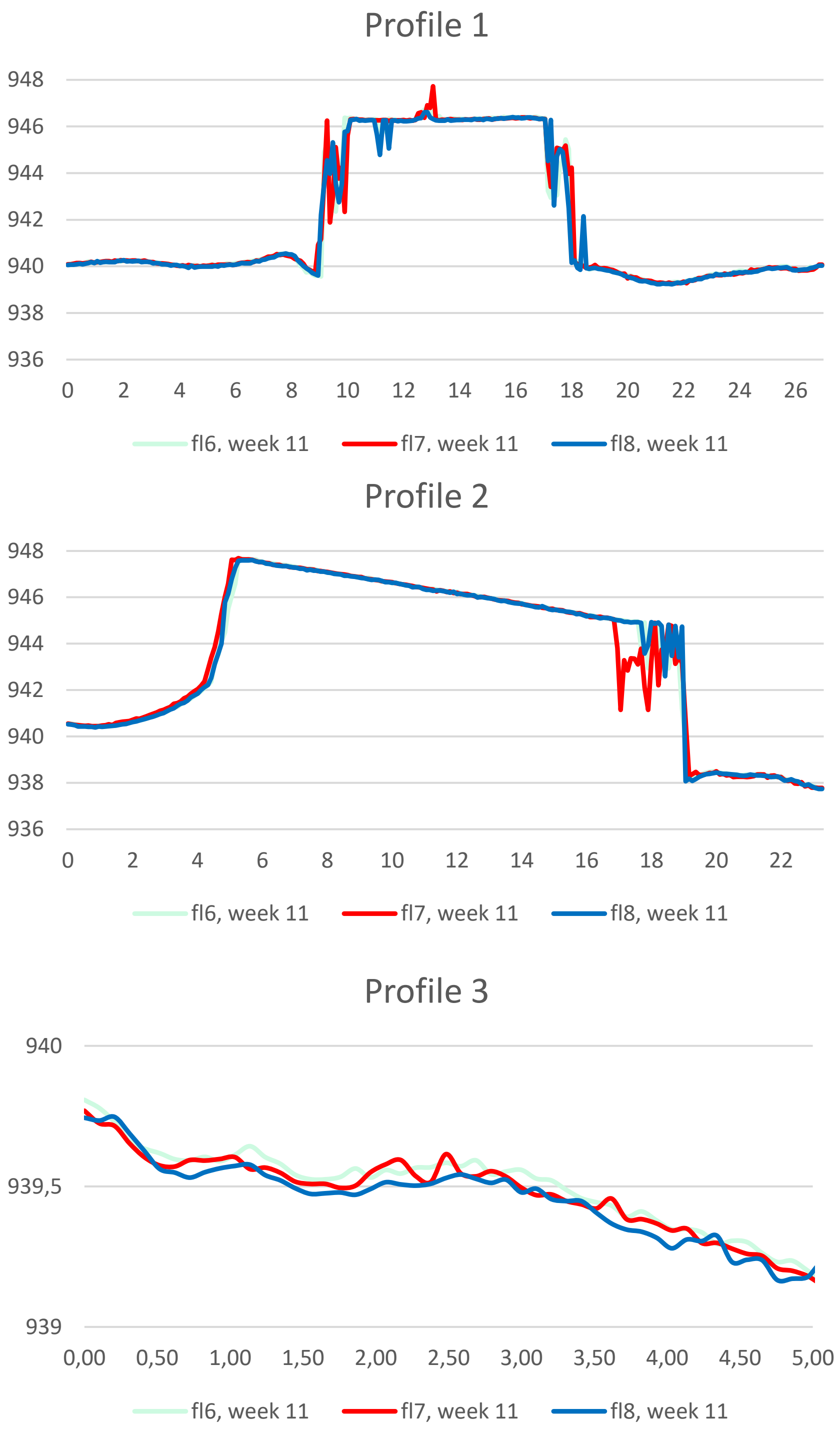

Figure 2.7.2-1: Flight profiles across and in front of Fonnbu research station. fl6 survey (green lines) was recorded with a 50 % LiDAR side overlap, fl7 survey (red lines) was recorded with a 35 % side overlap and fl8 survey (blue lines) was recorded with a 20 % side overlap. Horizontal and vertical scales are in m.

2.8 Vertical variability

To compare the vertical variability between different flights, five points were selected on the roof of the research station to extract height measurements. The location of the points are shown in Figure 2.8-1, and the extracted height values are given in Table 2.8-1: Extracted height in m.a.s.l. for the 5 points, for all the Since the datasets were collected in two rounds throughout the day, the statistics for fl1-5 surveys are displayed in Table 2-8 and for fl6-8 surveys in Table 2.8-3. For both the results presented in Table 2-8 and Table 2.8-3, we observe that the measured values range is within less than 0.1 m. The survey parameters given in Table 2-8 have a larger range than those in Table 2.8-3. This might be due to the larger number of flights in Table 2-8 which have been collected over a longer time period than the three flights in Table 2.8-3.

Figure 2.8-1: Location of reference points on the roof of Fonnbu research station where height values are extracted from each flight.

Table 2.8-1: Extracted height in m.a.s.l. for the 5 points, for all the surveys.

Survey	pt. 1	pt. 2	pt. 3	pt. 4	pt. 5
fl 1, week 11	945.27	945.18	947.66	947.47	946.19
fl 2, week 11	945.32	945.25	947.71	947.51	946.26
fl 3, week 11	945.30	945.19	947.68	947.48	946.22
fl 4, week 11	945.33	945.25	947.71	947.51	946.25
fl 5, week 11	945.35	945.26	947.73	947.54	946.27
fl 6, week 11	945.36	945.30	947.76	947.53	946.31
fl 7, week 11	945.36	945.27	947.76	947.57	946.30
fl 8, week 11	945.33	945.24	947.70	947.52	946.25

Table 2.8-2: statistics of extracted heights for fl1-5 surveys.

	pt. 1	pt. 2	pt. 3	pt. 4	pt. 5
Mean Value	945.32	945.22	947.70	947.50	946.24
SD	0.028	0.032	0.025	0.023	0.028
Range	0.08	0.08	0.07	0.07	0.08

Table 2.8-3: statistics of extracted heights for fl6-8 surveys.

	pt. 1	pt. 2	pt. 3	pt. 4	pt. 5
Mean Value	945.35	945.27	947.74	947.54	946.29
SD	0.016	0.025	0.029	0.024	0.025
Range	0.04	0.06	0.06	0.06	0.06

2.9 Influence of equipment and flight height

From day-to-day LiDAR scans of the same avalanche release areas, differences that could not be explained by natural changes were found when comparing DEMs derived from two different DJI L1 LiDAR scanners. Similar differences were found using each of the LiDAR sensor to scan the same area close to Fonnbu with the exact same flight and survey settings, just a few minutes apart. The vertical differences between the two derived DEMs (Figure 2.9-1, right) are on the scale of 10-20 cm within a few tenths of meters and indicate systematic errors that seem to be related to the distance from the ground to the flight lines. Similar errors were also found comparing two surveys of the same area at Tyinstølen (Figure 2.9-1, left), using the same LiDAR scanner but different flight height (80 and 60 m).

These findings show that the repeatability of surveys made with the DJI L1 LiDAR scanner can drop significantly when changing the equipment or the flight height. The reason for this is not known and should be investigated further. When using the L1 sensor to monitor changes over time, such systematic errors can be minimized by using the same equipment and the same flight height and survey settings for each survey.

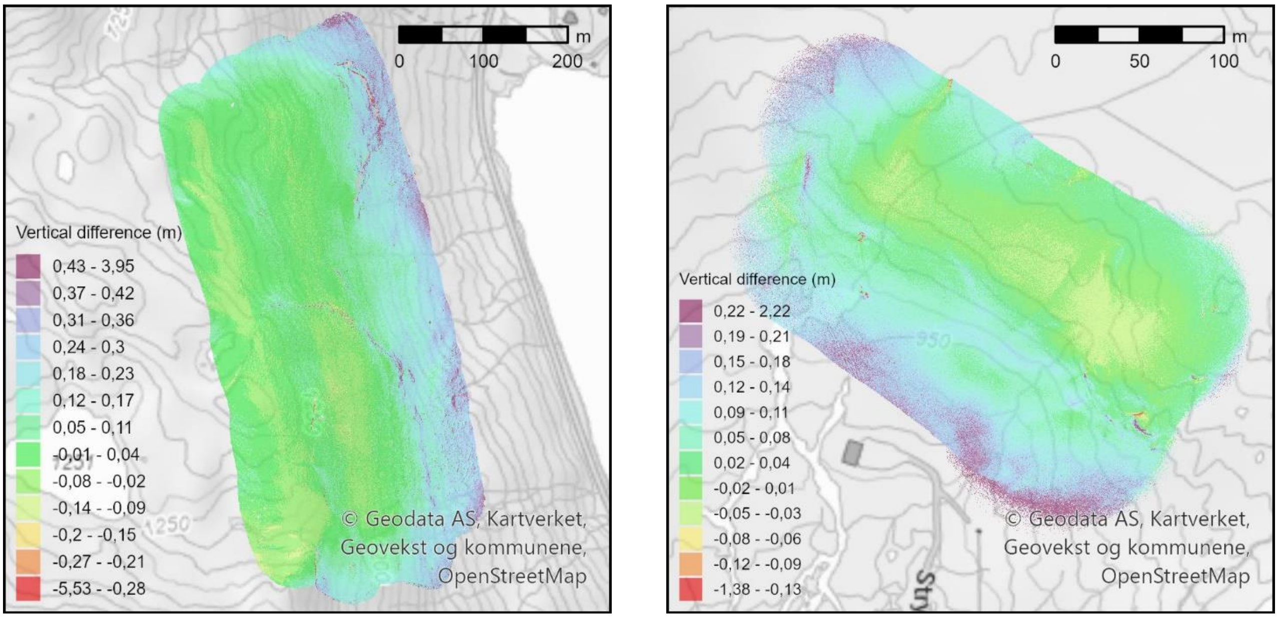

Figure 2.9-1: Left: vertical difference between DEMs derived from LiDAR scans at 80 and 60 m height at Tyinstølen recorded on Feb. 17th, 2023. Right: vertical difference between DEMs derived from LiDAR scans using different LiDAR payload with identical flight and survey settings at Fonnbu recorded on March 1st, 2023.

2.10 Comparison of LiDAR-derived snow height to snow height measurements with a snow probe

This section compares LiDAR-derived snow height to a snow height map created by interpolating from snow probe measurements. The location for this test was south of Fonnbu research station (Figure 2.10-1, left). Only the four edge points of the survey area were georeferenced, hence there is uncertainty concerning the exact location of each individual point. Based on the known outer frame, i.e. of the edge points, and the knowledge that the measurements had a 10 m x 2 m spacing, the points were logged as displayed in Figure 2.10-1 (right). High spatial variability due to presence of boulders and small creeks was also observed during snow probing.

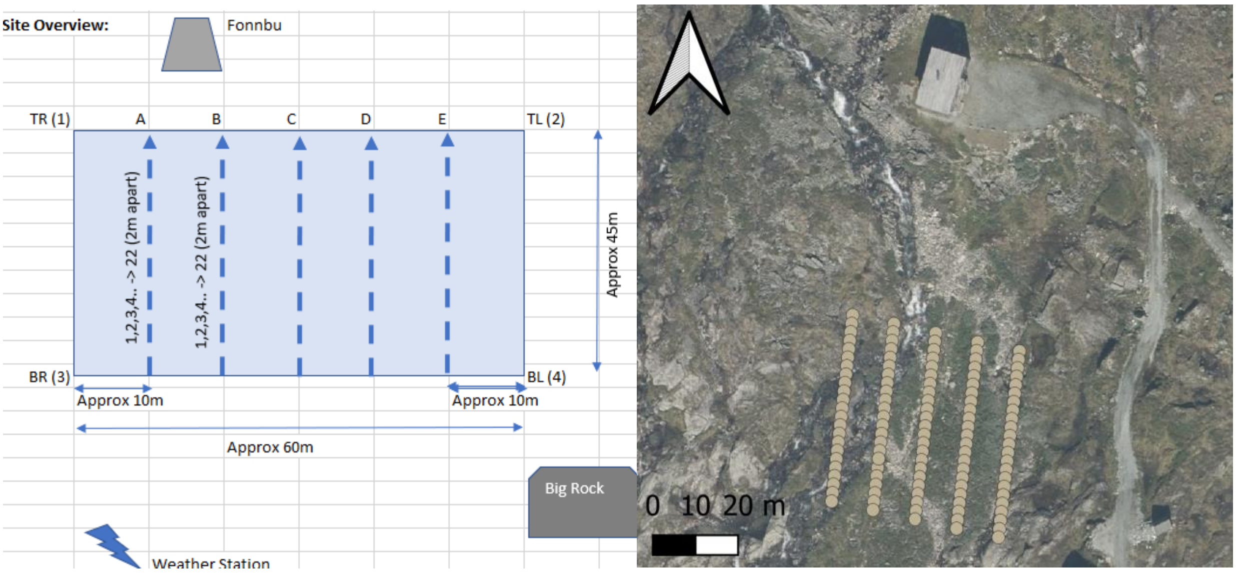

Figure 2.10-1: Left: conceptual scheme of the snow probing measurement set-up. Right: location of the measurements south of Fonnbu research station.

Triangulated Irregular Network (TIN) interpolation was used in QGIS on the gridded data to create a snow height map. When selecting the pixel size for the created raster, two different resolutions have been tested: 2 m (Figure 2.10-2) and 0.5 m (Figure 2.10-3). We compared the snow probe snow height map with the snow height map derived from flight recorded on week 9 (see Table 2.1). This LiDAR snow height map was resampled and aligned in order to fit the resolution to snow-probe derived snow height maps.

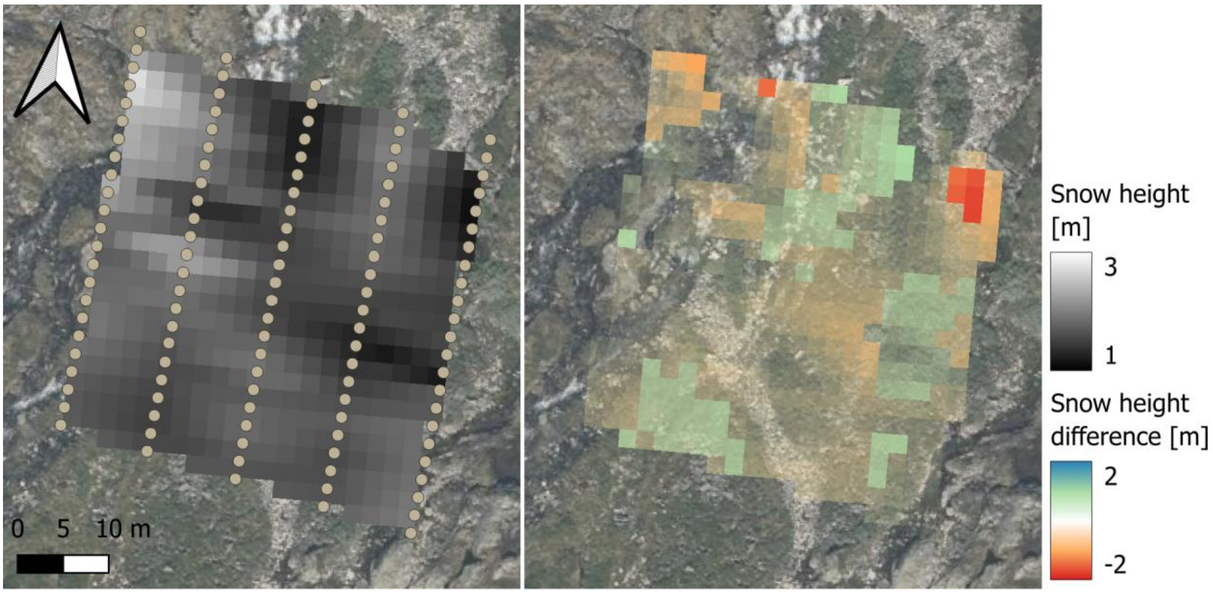

Figure 2.10-2: Left: snow height map with a 2 m x 2 m resolution, created with Triangulated Irregular Network interpolation from snow probe measurements. Right: snow height difference map between the TIN interpolated snow height map and the snow height map derived from LiDAR scan on week 9.

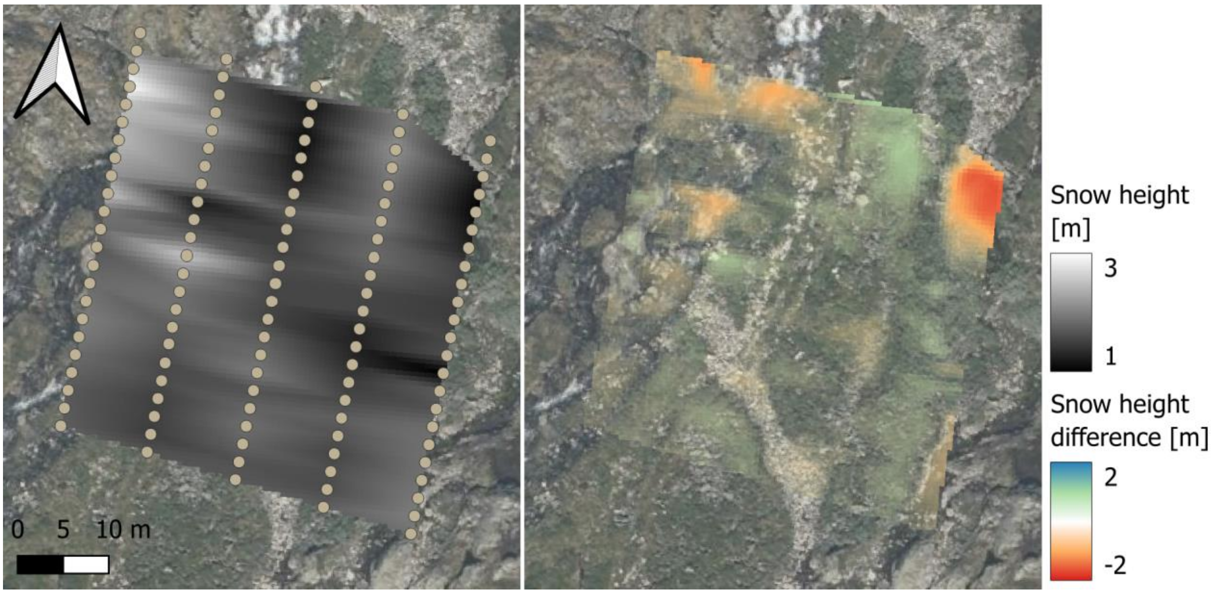

Figure 2.10-3: Left: snow height map with a 0.5 m x 0.5 m resolution, created with Triangulated Irregular Network interpolation from snow probe measurements. Right: snow height difference map between the TIN interpolated snow height map and the snow height map derived from LiDAR scan on week 9.

Comparing the snow probe snow height map to the collected LiDAR data on week 9 has certain limitations, since the exact location of the snow probe measurements is not perfectly known. However, in general it can be assumed that the use of a quite dense net of snow probe measurements and their interpolation yields a realistic snow height map. Comparison to the snow height map from week 9 shows that the difference between the two maps is within ± 2 m and mostly much better, with the biggest deviations of -2 m in areas close to the edge of the measurement frame. However, to really evaluate the accuracy of LiDAR-based snow height maps, one needs to repeat the test with properly georeferenced in-situ measurements.

3. Photogrammetry part

3.1 Motivation

Photogrammetry is a well-established technique to build digital elevation models (DEMs) and point clouds from optical UAS data. Extensive literature is available, and we refer to the review papers of Bühler et al.[1,2]. In this report we focus our work on the following points:

- Estimating the margin of error for repetitive UAS surveys over snow with a medium-to-large image dataset relative to a reference dataset, by visual and statistical analysis.
- Comparing different methods and software, and benchmarking these against a reference dataset.
- Comparing two different UAS platforms over the same area.
- Assessing computational resource requirements and method efficiency from data capture to model production.

3.2 Summary and observations

The photogrammetry work demonstrates that both GCP and RTK-based methods can produce accurate and repeatable DEMs over snow covered surfaces. The workflow using Open Drone Map (MOD_ODM) and Sitescan software provided the most consistent results, with minimal deviations and high depth resolution. While there were some georeferencing errors with the Datact software, overall, the study showed that photogrammetry is a reliable technique for building detailed elevation models, especially when using high-end UAS platforms and appropriate processing software. The findings support the integration of photogrammetric methods into workflows for applications such as avalanche forecasting, where accurate terrain modeling is crucial. A short summary of the software packages used are described below.

3.2.1 Mod_ODM

- Includes a fully automated server-based workflow assembled by SINTEF, where images can be uploaded over an API-from a field computer. The software is based on open-source Python libraries and uses Open Drone Map (ODM) project[3] as the core photogrammetry processing library. The ODM software is itself based on several high-quality open-source projects, including the OpenSfM[4] structure from motion library and Micmac, and the multiview stereo reconstruction OpenMVS[5]. Client server pre-processing and post-processing code as well as the "one-click"-wrapper code are assembled in-house and uses additional open-source python libraries. Some more discussion can be found in Dupuy et al. (2024)[6]. As this workflow includes image preprocessing stages before it is sent to the odm-processing engine, we have chosen to call it this workflow Mod_ODM.

---

[1] Bühler, Y., Adams, M.S., Bösch, R. and Stoffel, A., 2016. Mapping snow depth in alpine terrain with unmanned aerial systems (UASs): potential and limitations. *The Cryosphere*, *10*(3), pp.1075-1088.
[2] Bühler, Y., Marty, M., Egli, L., Veitinger, J., Jonas, T., Thee, P. and Ginzler, C., 2015. Snow depth mapping in high-alpine catchments using digital photogrammetry. *The Cryosphere*, *9*(1), pp.229-243.
[3] https://github.com/OpenDroneMap/NodeODM
[4] https://github.com/mapillary/OpenSfM
[5] https://github.com/cdcseacave/openMVS/
[6] Dupuy et al., 2024. Photogrammetry and LiDAR from UAS in steep terrain, *Statens vegvesen rapporter*, 991.

- The workflow is divided up into a client part, which is a separate application that can pre-process images in batch by selecting the raw-image folder. The pre-processing part consists of batch image contrast adjustment (Contrast Limited Adaptive Histogram Equalization), followed by local images resizing and subsequent uploading to the ODM-server instance. The client application has access to result models when processing has finished. Different settings can be chosen based on quality criteria ensuring flexibility. This workflow enables "one-click" processing of a georeferenced image set.

Key Features:

- Preprocessing: Includes image enhancement techniques such as Contrast Limited Adaptive Histogram Equalization (CLAHE) to improve detail and contrast in images, particularly useful for snow-covered areas.
- Processing: Uses open-source project node-ODM, Structure from Motion (SfM) and Multi-View Stereo (MVS) algorithms to reconstruct 3D models from 2D images.
- Georeferencing: Capable of using both GCPs and RTK data for accurate georeferencing.
- Batch Processing: Supports parallel processing to handle large datasets efficiently.

Performance:

- Provided consistent results with minimal deviations in elevation profiles.
- High depth resolution and accurate model generation, especially when using the enhanced image preprocessing module.

3.2.2 Metashape

- A commercial software developed by Agisoft, widely used in the photogrammetry community.
- Known for its user-friendly interface and robust processing capabilities.

Key Features:

- Image Processing: Supports a wide range of image formats and provides tools for image alignment, dense point cloud generation, mesh construction, and texture mapping.
- Georeferencing: Can utilize GCPs, RTK data, and manual input for georeferencing.
- Customization: Allows users to adjust processing parameters to optimize model accuracy and quality.

Performance:

- Produced quality georeferencing with high accuracy.
- The model was slightly smoothed compared to Mod_ODM; and Sitescan, with less detail in depth resolution.

3.2.3 Sitescan

- A cloud-based photogrammetry solution by ESRI.
- Designed for ease of use and integration with Autodesk and ESRI software products.

Key Features:

- Cloud Processing: Offloads computational tasks to the cloud, allowing for efficient handling of large datasets.
- Automated Workflows: Provides automated image processing, model generation, and georeferencing.
- Collaboration: Facilitates sharing and collaboration through cloud storage and integrated tools.

Performance:

- Showed reliable results with minimal deviations in elevation profiles.
- Slightly noisier and more pixelated models compared to MOD_ODM, likely due to default settings used during processing.

3.2.4 Datact

- A commercial photogrammetry software used for generating 3D models and DEMs from aerial images.
- Focuses on high accuracy georeferencing and detailed model reconstruction.

Key Features:

- Advanced Georeferencing: Utilizes both GCPs and RTK data for precise model alignment.
- Customizable Processing: Offers a range of settings for optimizing image alignment, point cloud generation, and mesh construction.
- Error Correction: Includes tools for identifying and correcting georeferencing errors.

Performance:

- The model had a systematic georeferencing error of 40-50 cm, leading to significant deviations in elevation profiles.
- Despite this, it provided detailed models, though with larger deviations compared to MOD_ODM and Sitescan.

3.3 Reference model

3.3.1 Ground truth and ground control points

The ground truth (i.e., the assumed correct absolute position) of the created models relative to the ground, can be assessed based on using the available obtained ground control points as input to the modelling, instead of drone GNSS, for georeferencing. In theory, it is then only the 3D-model reconstruction errors that account for the model georeferencing errors. Photogrammetry with Real-Time Kinematic (RTK), using high end equipment and processing software with calibrated settings, should create consistent results, without the use of ground control points, with a vertical average deviation across the model of about +-5 cm's, depending on terrain steepness.

The RTK-generated models are compared to this "ground truth model" to assess the accuracy of the GNSS-generated models. The ideal result should be as close to the assumed ground truth model which gives an idea of the accuracy of the GNSS-generated models.

Using direct control points without GNSS also has errors due to manual tagging of pixel areas on images, which is prone to inaccuracies. For example, each image containing GCP's in the image dataset has its recorded pixels on each raw image prior to processing. There may be deviations in the creation of the references.

3.3.2 Reference model for the M300_Breiddalen#1 dataset

The M300_Breidallen#1 dataset was acquired in Breiddalen, Norway, by NPRA using a DJI M300 RTK. A similar survey with a DJI Phantom 4 Pro by NGI provided two sets of data for analysis. All ground control points created were used in the photogrammetric processing for creating the reference model of the M300_Breidallen#1 set.
All GCPs created were used in the photogrammetric processing for the reference model. Mod_ODM, was used to analyze the reference dataset.

Example ground control points
In the figure below, the ground control points are shown for the survey area. The GCP's are tagged to the raw images using the open-source project GCPEditorPro[7]. Points B11 and B4, located on the edge of the area, only had two tagged images, which is a bare minimum (see Figure 3.3.2-1). All other points contained from 3 to 8 images. Six GCP's contained 3 tagged images. A total of 19 GCP's were used.

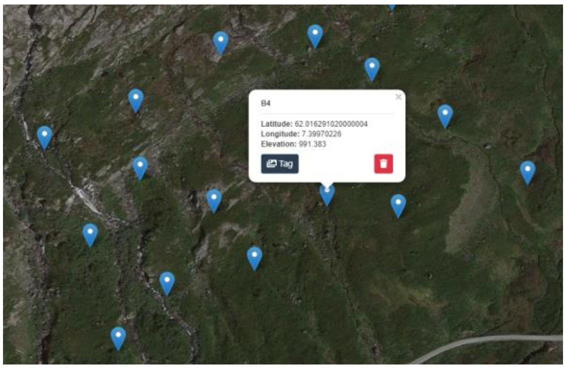

Point B4

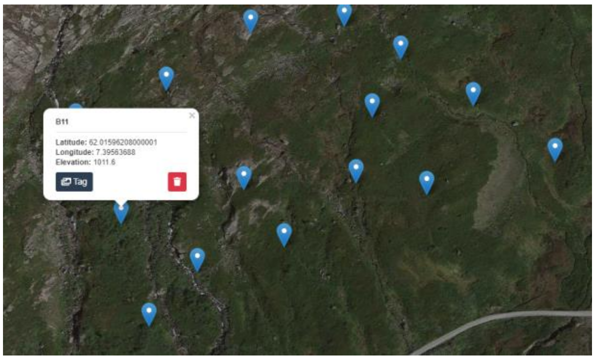

Point B11

Figure 3.3.2-1: GCP's of the survey region. Certain ground control points along the edge of the survey area were only found in three overlapping raw images.

The original image set was tagged with no pre-processing (adaptive histogram adjustment). This results in some reduced detail and resolution, especially over larger areas of similar snow surface. The optimized images would require its own tagging, which was not done for the reference set. The images were also resized depending on compute and processing time. As the surveyed elevation coordinates were used, no vertical re-projection (NN2000) is needed as with the cases where the reference (no-snow) elevation model is used. Three different settings were used with different resolutions: low, medium, and high.

[7] https://github.com/uav4geo/GCPEditorPro

Selected GCP's visual errors in x/y direction

For visual comparison with the ground control points, orthophotos are required accompanying the elevation models (Figure 3.3.2-2).

Figure 3.3.2-2: Orthophoto with visual GCP's Breiddalen#1 dataset (DJI M300 RTK), made with the MOD_ODM procedure

Point B18, three images with the GCP

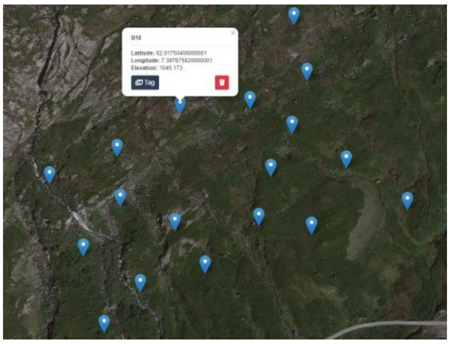

Point B18

Point B16, 8 images with the GCP
(5.6 cm from center)

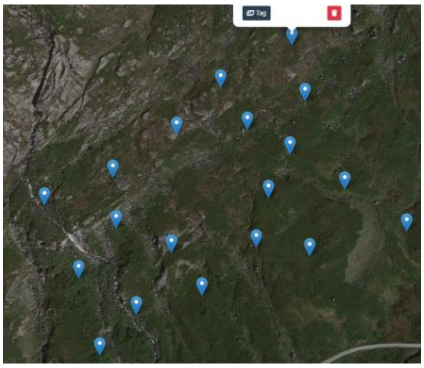

Point B16

Point B10, seven images with the GCP

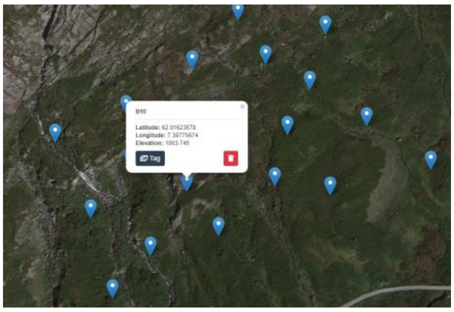

Point B10

Figure 3.3.2-3: Example close-ups of the model created using selected GCP's.

From the close-ups (Figure 3.3.2-3), one can see that there are some distance errors at the points in the centimeter range. Any error can also be due to inaccuracies in the manual tagging process. It can also be due to inaccuracies during image reconstruction. In Figure 3.3.2-4, the same positions are shown with the reference RTK-model (using the open-source model setup with pre-processing). The distance error from center is in the same range (< 10 cm). A diagonal across the model measures a distance of 660 m, indicating a horizontal model error of 660 +- 0.04 meters.

Point B18, RTK

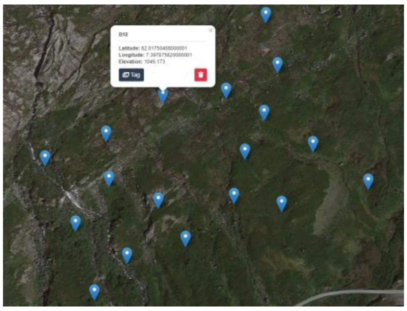

Point B18

Point B16, RTK.
Distance from center 0.088 m

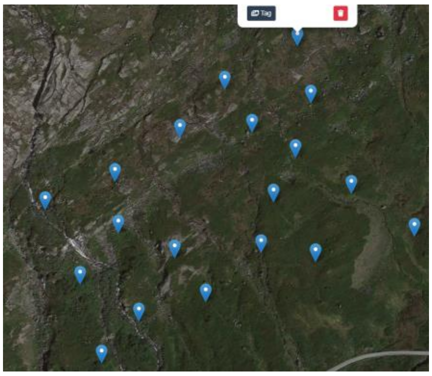

Point B16

Point B10, RTK

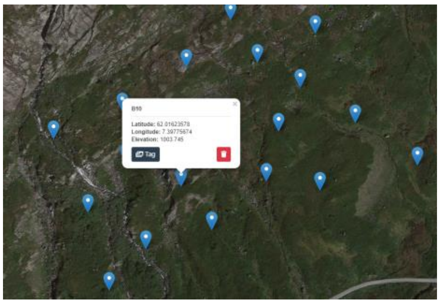

Point B10

Figure 3.3.2-4: The processed dataset Breiddalen#1 (DJI M300 RTK), using the drones internal positioning RTK. Thus, in the figure the orange control points are placed on the orthophoto after processing.

Elevation transects with 1-GCP's 2-Internal navigation M300, 3-internal navigation Phantom 4

To compare the differences in results for the elevation models, a transect was arbitrarily made through the three reference DEM's (Figure 3.3.2-5). This gives a qualitative understanding of the accuracy and deviation between the models. The red dot shows where the elevation differences are measured, and it is also arbitrarily chosen. The y axis shows an absolute difference of less than 4 centimeters for the given point (Figure 3.3.2-6). Figure 3.3.2-7 and Figure 3.3.2-8 give selected parts of the transect crossing the location of one GCP and data recorded with a DJI Phantom 4 Pro drone (Figure 3.3.2-8).

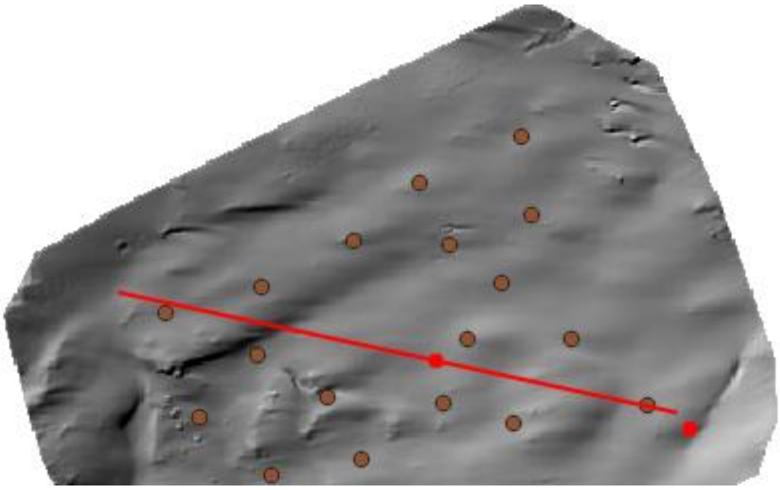

Figure 3.3.2-5: Transect location through the DEMs, processing using QGIS 3.24.

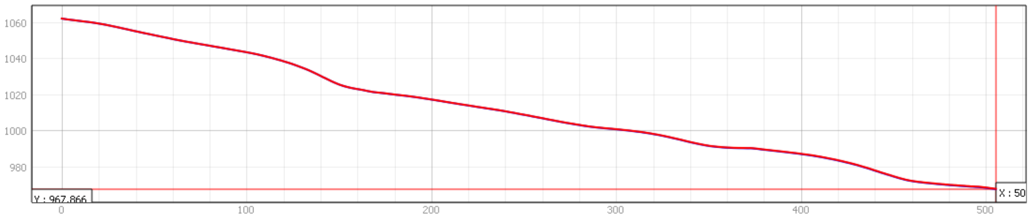

Figure 3.3.2-6: Elevation profile over the full transect, x- and y-axis in meters.

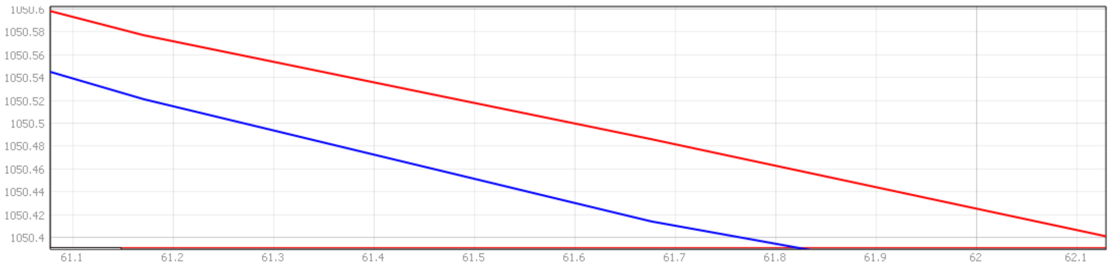

Figure 3.3.2-7: Selected part of elevation profile. Deviations of +/-2 cm along the transect. Red line: RTK georeferencing. Blue line: GCP georeferencing. x- and y-axis in meters.

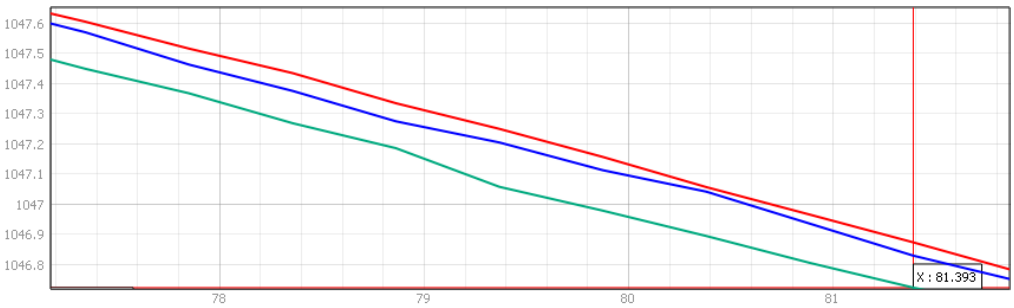

Figure 3.3.2-8: Part of elevation profile. Deviations of +/-6 cm along the transect. Red line: RTK (Breiddalen#1 dataset, DJI M300). Blue line: GCP georeferenced (Breiddalen#1 dataset, M300. Green line: Breiddalen_Phantom_pro4). x- and y-axis in meters. Processing done with the open-source workflow.

Processing summary for the reference Breiddalen#1 dataset

From the analysis of the reference model errors during reconstruction, which is georeferenced with GCP's, There are two types of errors of interest, the error of the expected georeferencing accuracy relative to the RTK values of the photos, and the point colud error, giving relative accuracy of the reconstruction for the compared model. For the georeferenced errors, it is shown that the vertical errors are the largest with an absolute and relative accuracy of 22 cm and 6 cm, respectively. Horizontal errors are lower at a few cm's for this case. Note that for the same set but with georeferencing using RTK, the relative vertical error is similar at +/-5 cm.

3.4 Comparison of different processing software using the Breiddalen#1 M300 dataset

Independent models were produced using the same image set from MOD_ODM, Metashape, Sitescan, and Datact software. Models were RTK georeferenced without GCPs. We use the Breidalen#1_M300 survey dataset for this analysis.

3.4.1 Visual comparisons of orthophotos

From the visual comparison, the RTK generated models have reference markers that are in the center for each ground control point, showing high horizontal accuracy (Figure 3.4.1-1, Figure 3.4.1-2, Figure 3.4.2-1).

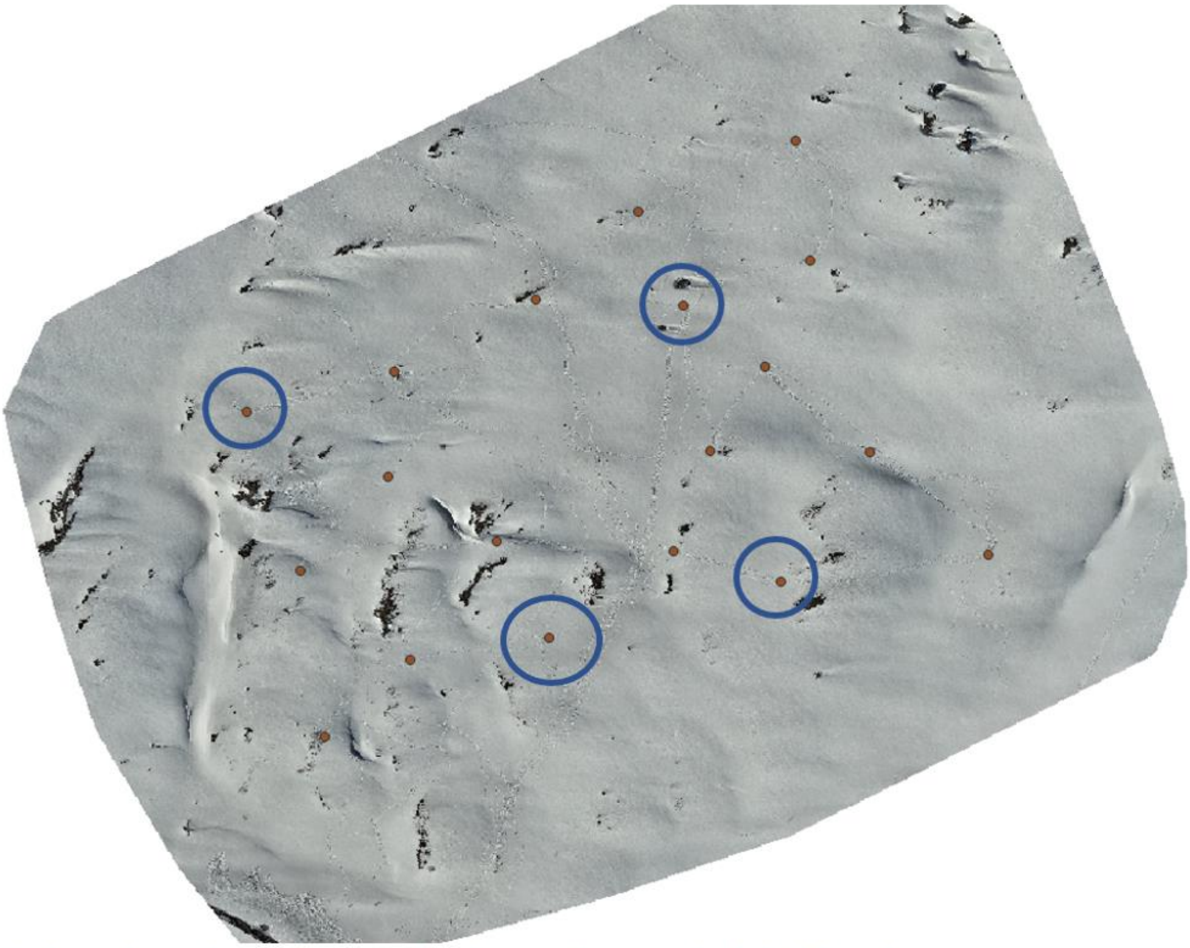

Figure 3.4.1-1: Orthophoto with control points. Four points have been visually compared with the different datasets. Points A, B, C and D are located at the top left, top right, bottom left and bottom right

of the model. Close ups are given in Figure 3.4.1-2 compared to Metashape. This particular orthophoto is created with MOD_ODM.

MOD_ODM software w/preprocessing engine	Metashape (low resolution version)
	
	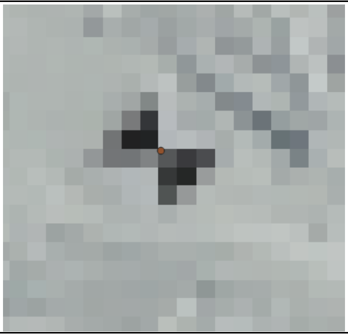
	
	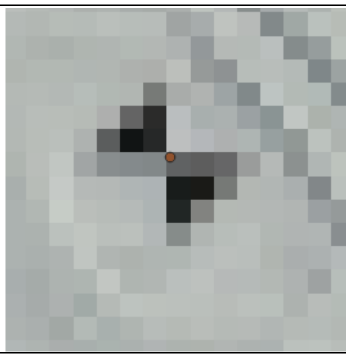
Points mostly well centered	Points mostly well centered

Figure 3.4.1-2: Example close-ups of the orthophotos around control points. From top to bottom: A, B, C and D. The locations of the four control points are given in Figure 3.4.1-1. The left column gives the results for the opensource method while the right column gives the results for the Metashape model. Note that the resolution is not of interest here, but rather the correct location of the GCP's. The Metashape model was not run with higher resolution as a choice.

3.4.2 Terrain profile comparisons for the 4 software packages

The terrain profile tool in QGIS compares elevation precision amongst the different models created. An arbitrary transect was selected throughout the model and the elevation profiles of the surface are compared (Figure 3.4.2-1).

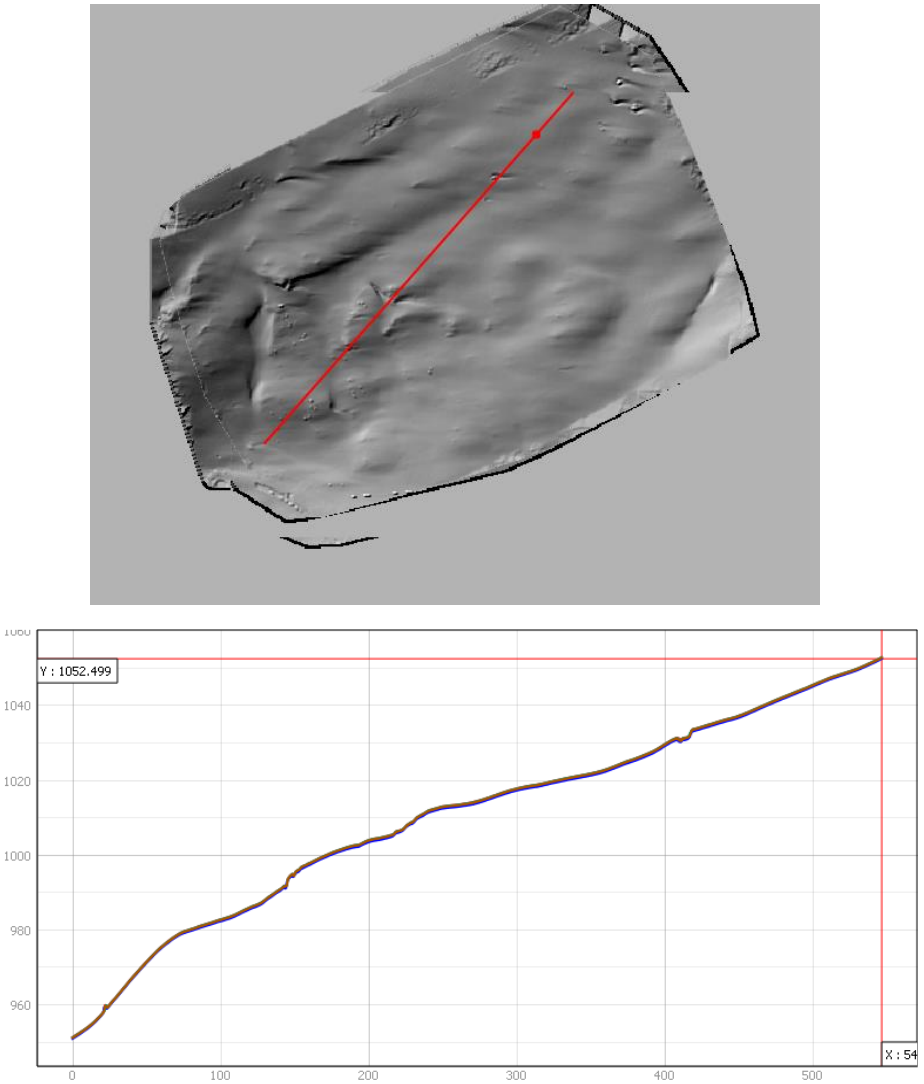

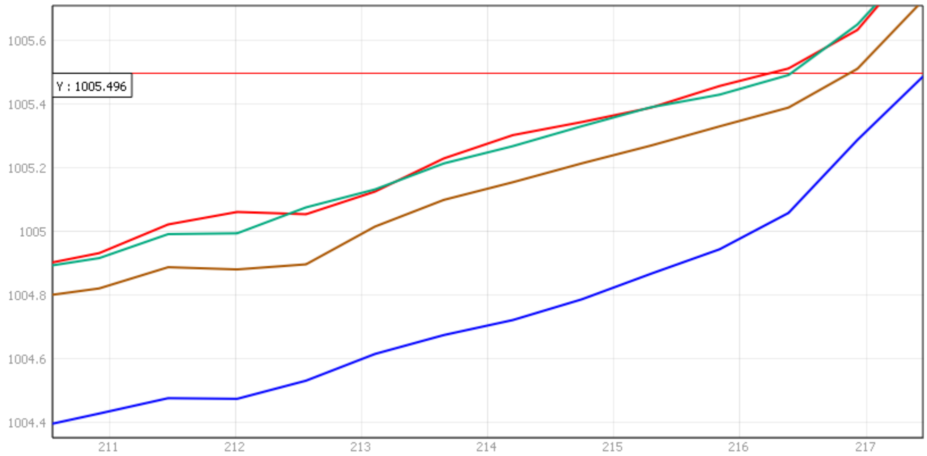

Figure 3.4.2-1: Top image: location of the transect shown on the DEM model. Middle image: elevation profiles of the transects for all models. Bottom image: arbitrary close-up view of the elevation profile between x=210 and x=218 meters. Red Line: MOD_ODM software, Green Line: Sitescan, Brown Line: Metashape, Blue Line: Datact. The y-axis ranges from 1004.4-1005.6 meters.

Observations:

- The Datact model (blue line) shows a clear systematic deviation of about 40-50 cm below compared to the other three models. This discrepancy is likely due to georeferencing errors, which can be verified by analyzing the orthophoto.
- When excluding the Datact model, the remaining three models (MOD_ODM, Sitescan, and Metashape) exhibit a deviation of about 15 cm.
- Between the MOD_ODM software and Sitescan, the deviation is minimal, only a few centimeters.

In Figure 3.4.3-2, the reference model, which was created using the Ground Control Points (GCP) directly, is represented by the black line (open-source model). The turquoise line, representing the model produced using Sitescan, closely matches the black line. While it is unclear which model has the highest accuracy relative to the actual ground truth, it is reasonable to assume that the model created with the GCP (black line) has a high degree of absolute accuracy.

3.4.3 Hillshade slice comparisons

The terrain profile tool available in QGIS was used to compare elevation precision amongst the different models created. Figure 3.4.3-1 shows slices of the orthophoto and DEMs processed with different software. A transect was made throughout the models (Figure 3.5.2-1).

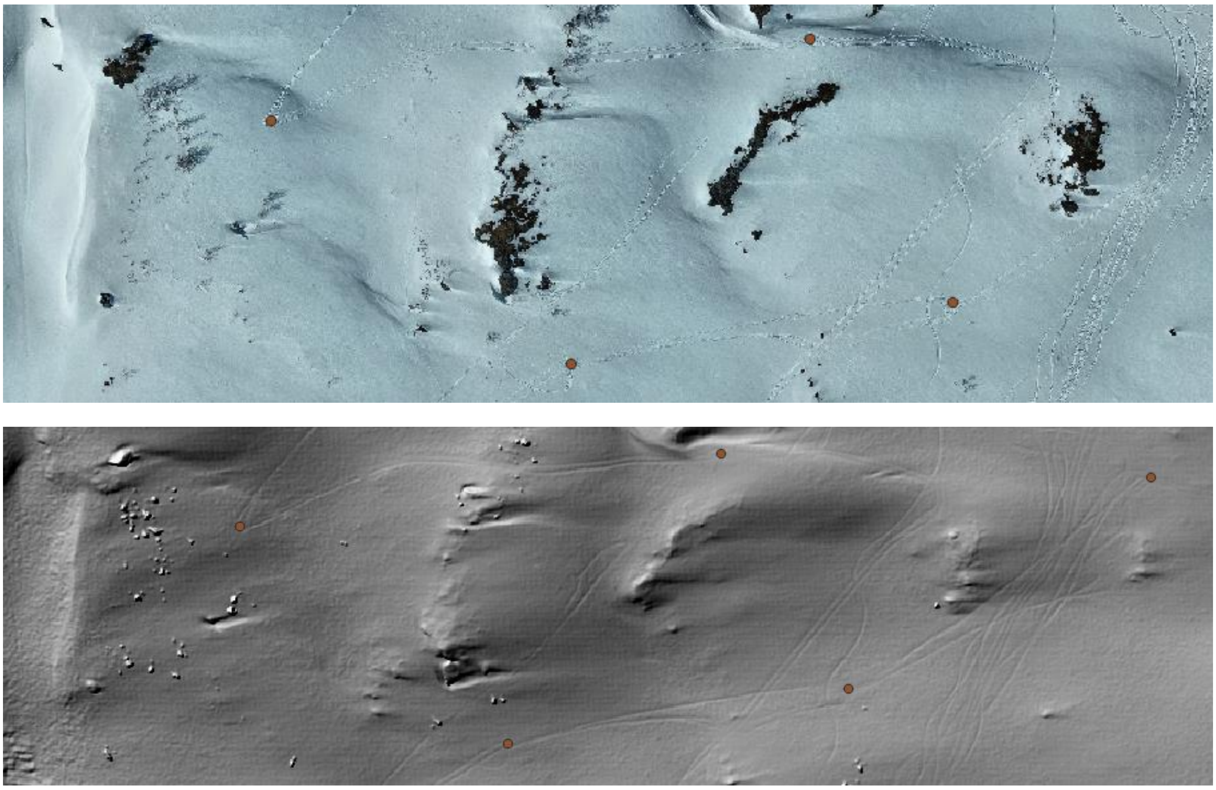

MOD_ODM ortho and DEM

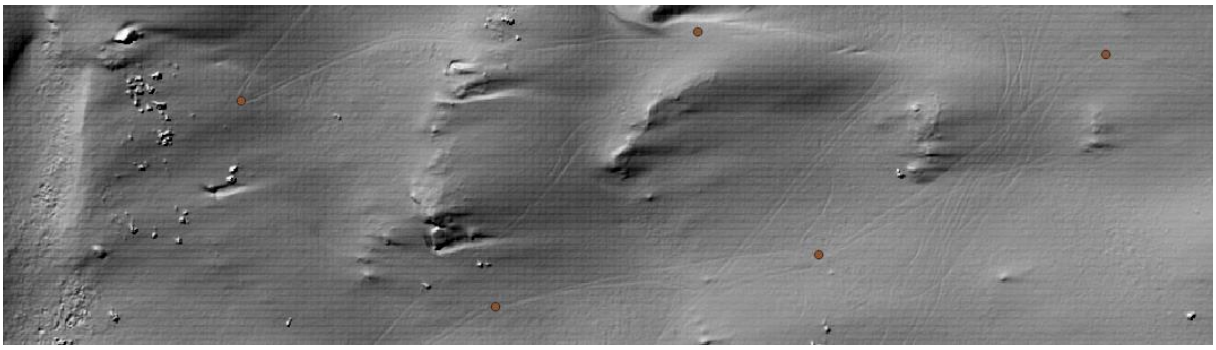

Datact

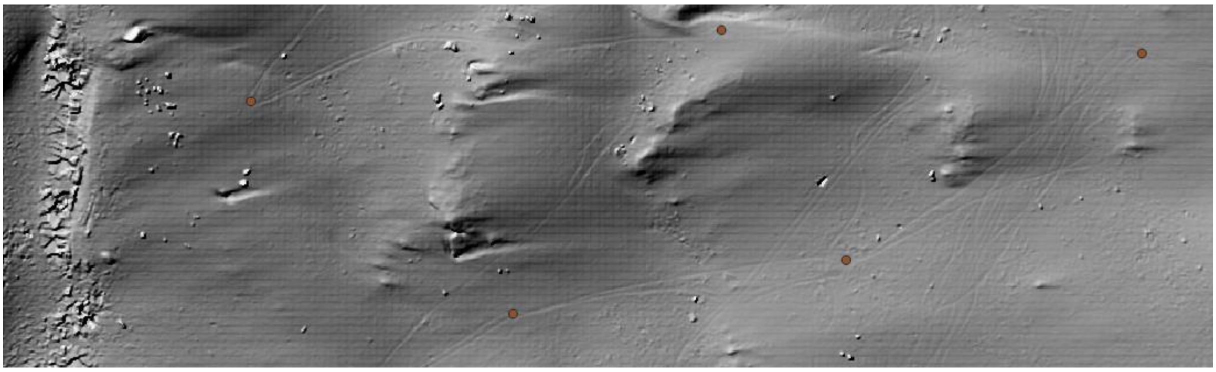

Sitescan

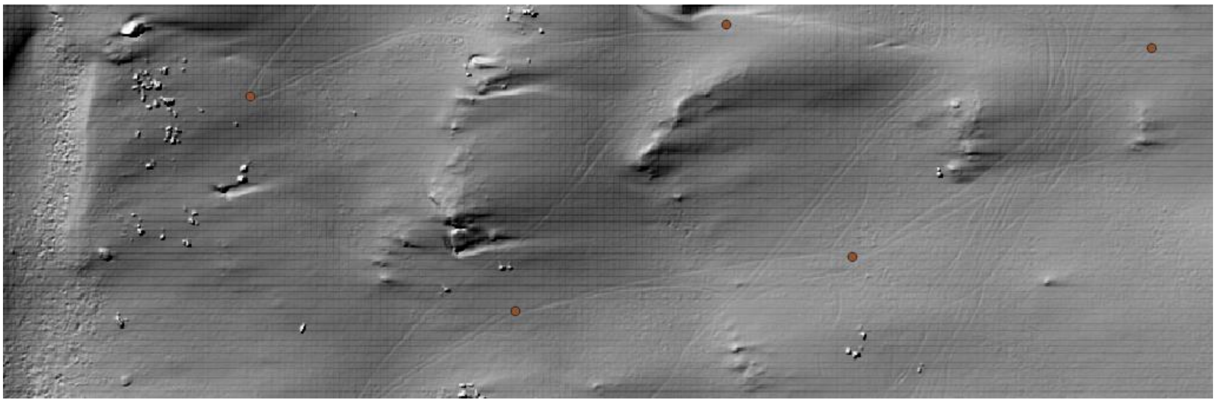

Metashape

Figure 3.4.3-1: Slices of a given section of each DEM for visual comparison processed with different software.

A part of the model was cut out as shown in Figure 3.4.3-1. Visually from the Hillshade one can see that their models from MOD_ODM software and Datact produce elevation models with little artifacts. A frequency domain analysis of photogrammetry dataset could be used to assess targets and artefacts. There are large areas with artifacts seen in the Sitescan model, especially on the left side, and less in the Metashape model, although still significant. One can see from the orthophoto that this area has clean snow, with an absence of rocks and other formations. Consequently, there should be no noise or artifacts here but only smooth surface. These artifacts were also initially seen with the MOD_ODM software, prior to implementing the pre-processor image enhancing routines (see appendix 1). This pre-processor automatically enhances the image quality, increases the size, and creates images with significantly more detail and contrasts. Therefore, large areas of the models from Sitescan and Metashape are here rendered non-usable for snow layer thickness calculation.

We consequently recommend using the pre-processor routine, also when using the commercial photogrammetry packages. The pre-processor runs in batch mode, multi-threaded, and takes approximately 10 minutes to run for a set of 400 images, on a laptop computer. Another sign to look for is the presence of ski tracks from the skiers setting up the GCP's. These should be clearly visible in the DEM's and contain no noise or artifacts. These visuals should also be set in relation to the system depth resolution settings.

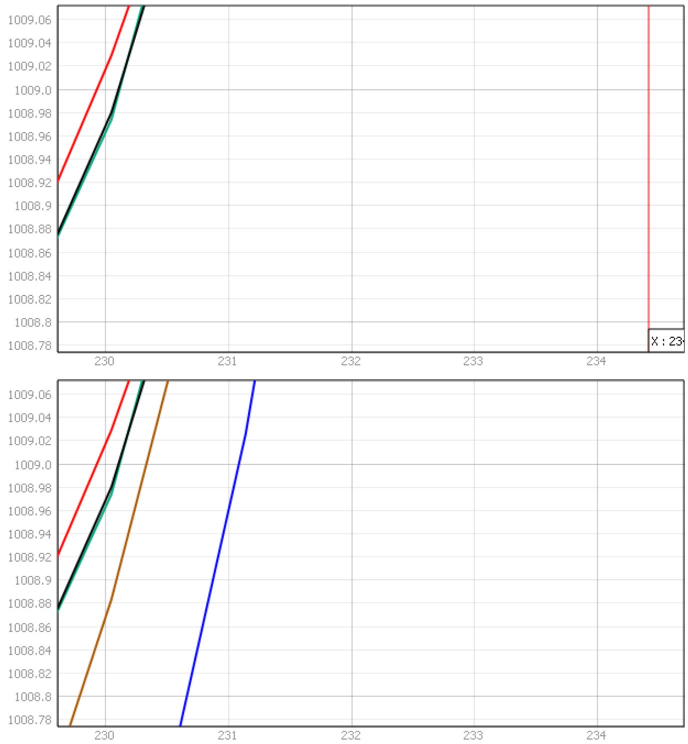

Figure 3.4.3-2: Zoomed-in view of a steeper region along the transect from Figure 3.4.2-1. The lines represent results from different software tools: red for MOD_ODM, green for Sitescan, brown for Metashape, and blue for Datact. The black line represents the GCP model, which was also created using the MOD_ODM software.

SINTEF

3.4.4 Cars and depth resolution

A specific comparison of the profiles of the cars located at the road at the edge of the survey area is analyzed with specific emphasis on model depth resolution (Figure 3.4.4-1). The Breidallen#1 image set image set is used. The first observation is that the Hillshades looks smoother for MOD_ODM, Datact and Meetashape, while the Sitescan shows to be somewhat more pixelated and noisier. This may be due to the settings choices when generating each model. As visually shown in Figure 3.4.4-2, the Datact result (blue line) shows larger deviation because of the systematic georeferencing deviation as described earlier. Further zoomed-in analysis is shown Figure 3.4.4-3, where the last three cars on the right side are shown. These cars are a good place for comparison, as the cars are discrete objects with vertical sides. In Figure 3.4.4-3, the middle figure shows the elevation profile of the car, comparing the different software's. The blue line representing Datact has been taken out. The lower figure in Figure 3.4.4-3 gives information of the numerical rate of contrast, i.e., the relative change in elevation along the transect over time. Larger peaks indicate larger vertical changes and higher resolution as higher peaks indicate higher density point cloud and better capture of the vertical sides of the cars. As the front and back of the car are immediate vertical elevation changes, the peaks in the slope plot should be as large as possible, indicating sharp depth resolution. The thickness of the "cutlines of snow" as results from the mowing machine should also be as thin as possible.

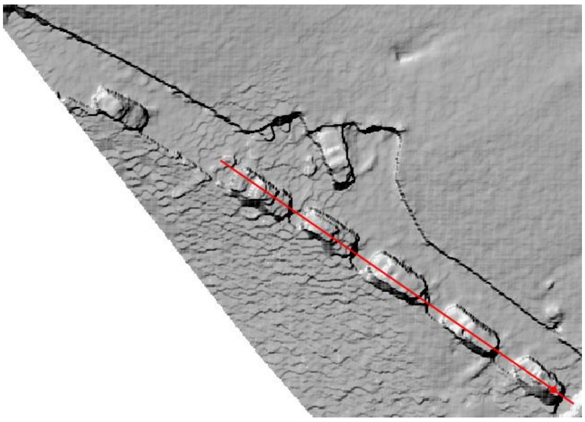

MOD_ODM

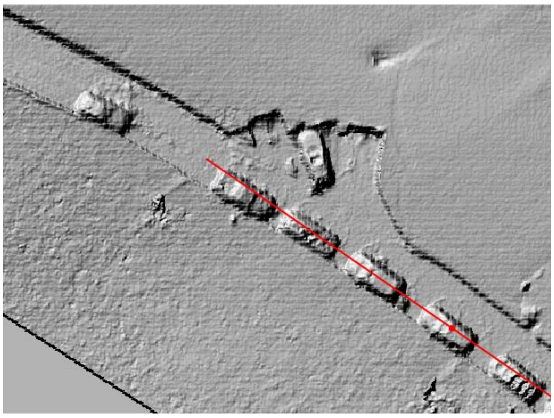

Datact

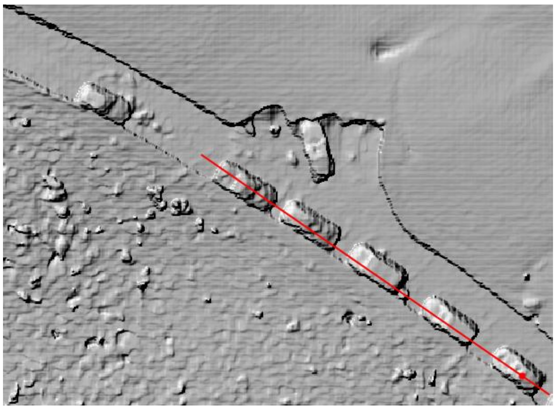

Sitescan

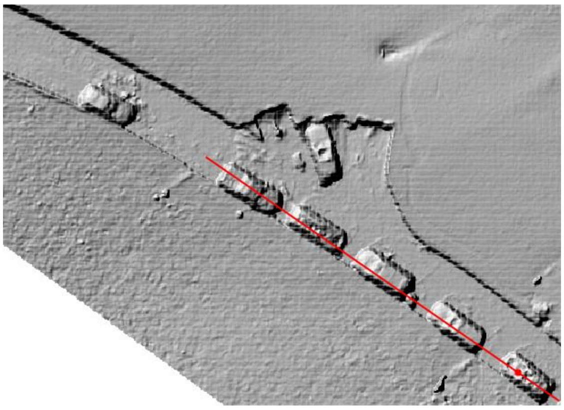

Metashape

Figure 3.4.4-1: DEM for the four different processing software's. The red line indicates the transect along the cars parked.

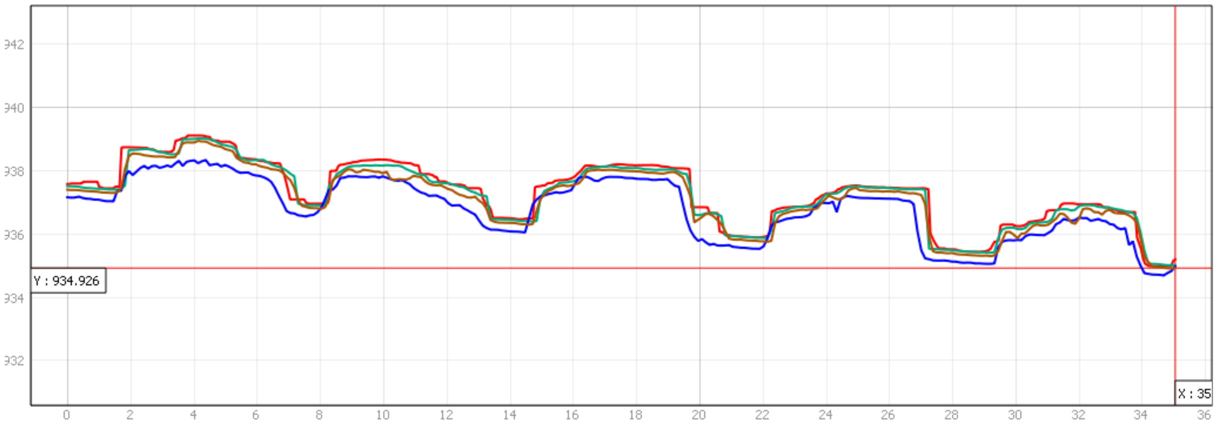

Figure 3.4.4-2: Profile of cars: Blue: Datact, Brown: Metashape, Turquoise: Sitescan, Red: MOD_ODM software. Slope with peaks showing the "sharpness" of the depth.

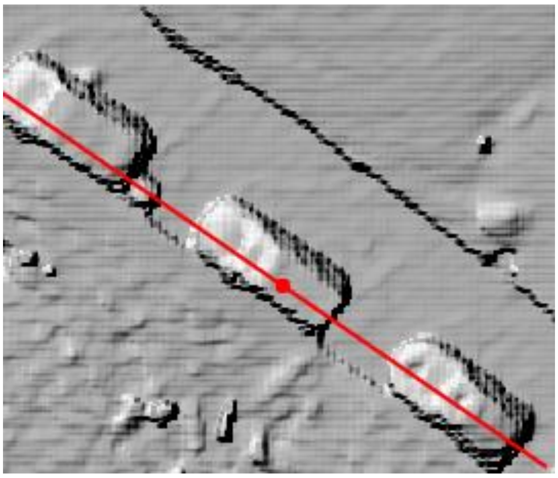

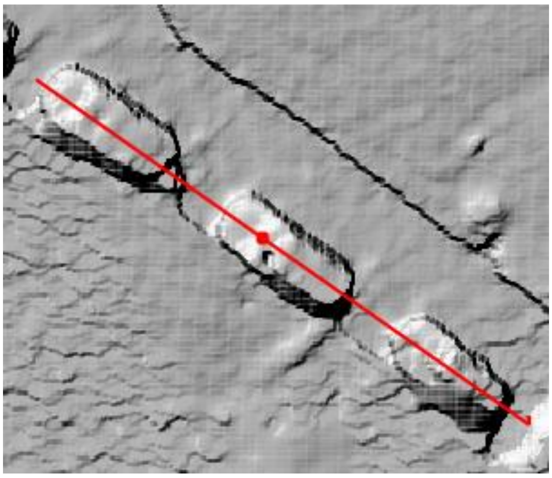

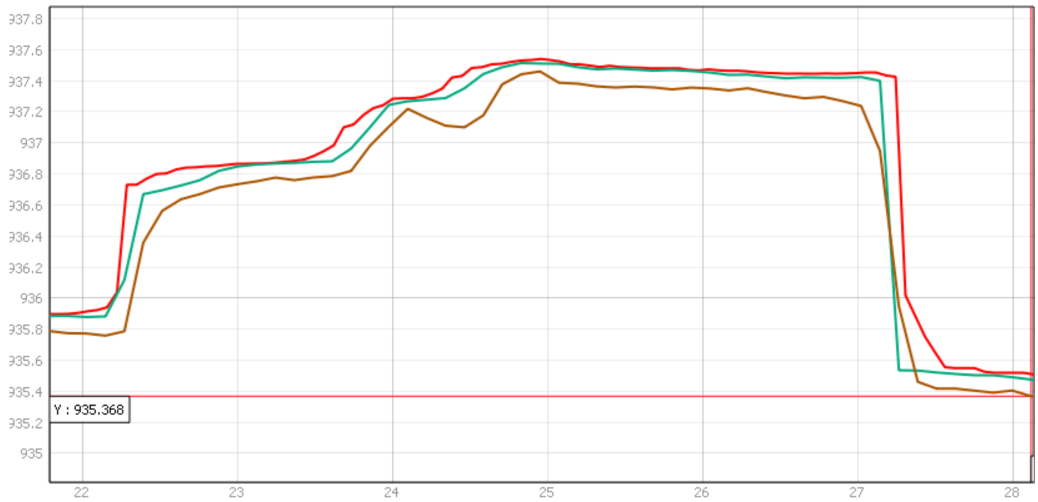

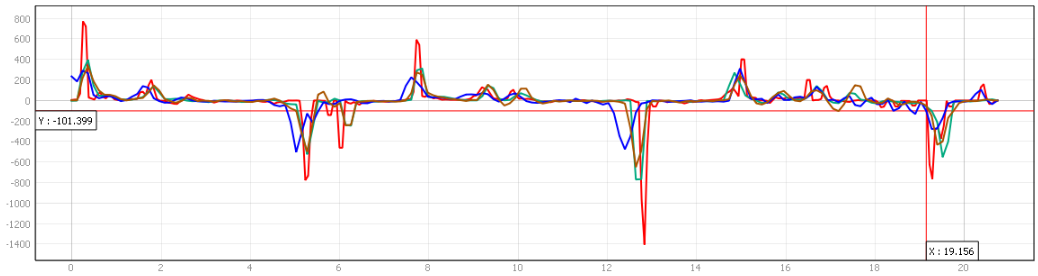

Figure 3.4.4-3: Profile of car: Blue: Datact, Brown: Metashape, Turquoise: Sitescan, Red: MOD_ODM software. Slope with peaks showing the "sharpness" of the depth. The larger peaks show higher depth resolution.

In Figure 3.4.4-4, a cross-section of the snow-edge, produced by the snow-mower, is displayed. This cross section is a cut vertical elevation step and may test the performance of the model in regard to depth resolution. The "thinner" the line separating the snow layer from the road, the higher resolution the model has. This is also shown by a larger slope change, represented by larger peaks. If specifically looking at the show-mower cut, which may give the most challenging reconstruction, as the snow-edge is almost a vertical cut, the Sitescan model and MOD_ODM software model are similar both in shape and location and point density. The Metashape model is slightly smoothed out and does not have the same point density as the two previously mentioned. The vertical height of this snow layer is at this point about 1 meter, and the RMS error for the open-source model in red is in the range of 5 cm. It should be noted that these results may be due to certain optimization settings, and the authors have not explored all options with the commercial packages.

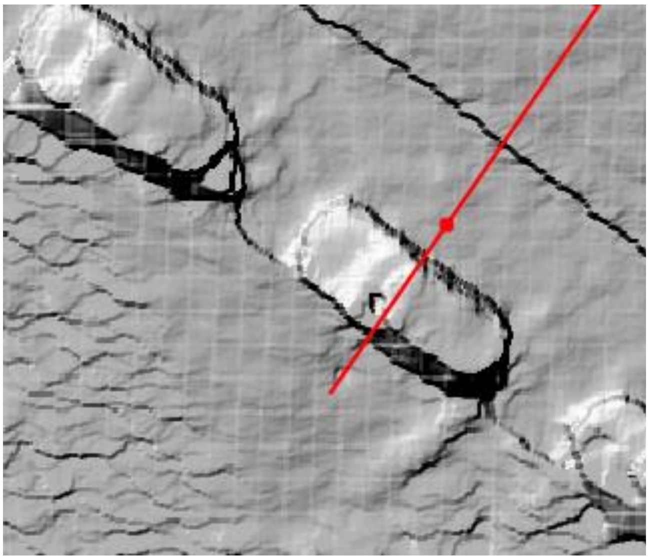

MOD_ODM

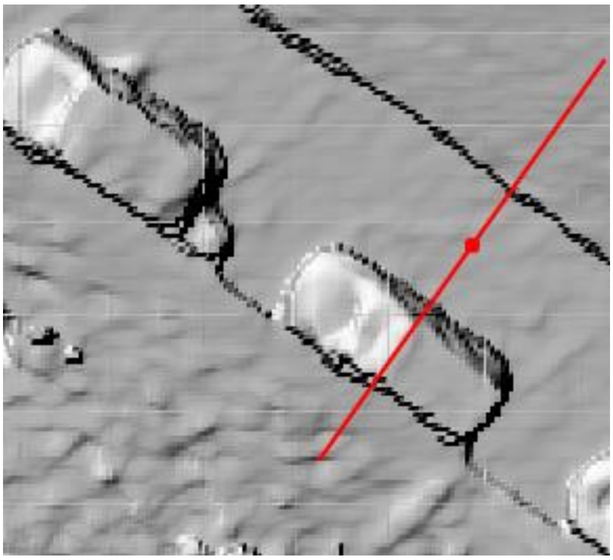

Sitescan

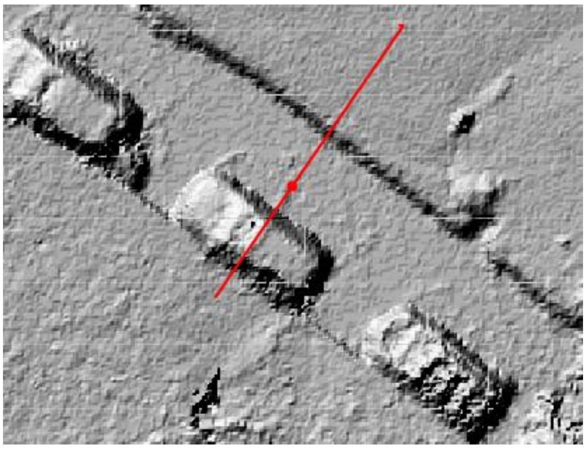

Datact

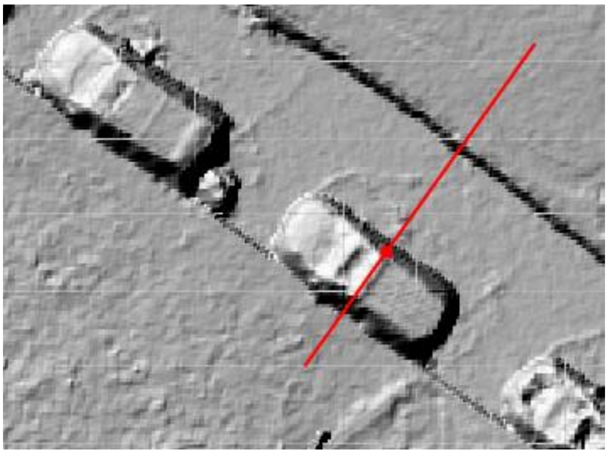

Metashape

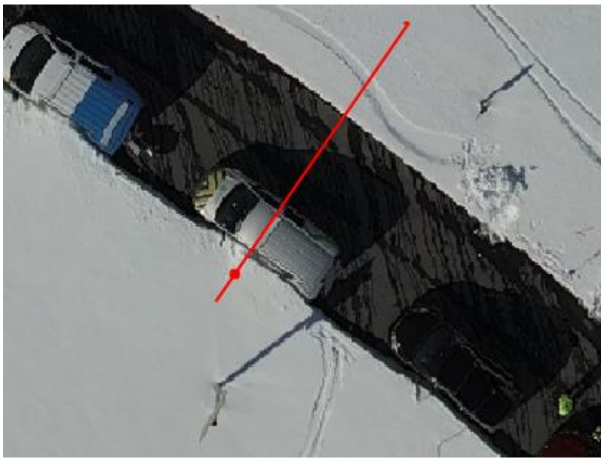

Orhtophoto (MOD_ODM default settings)

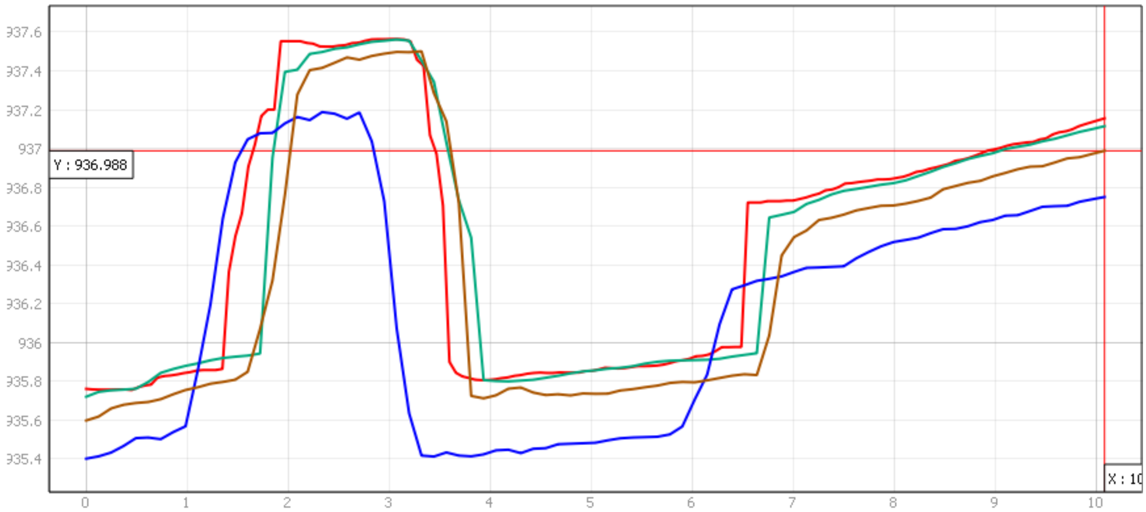

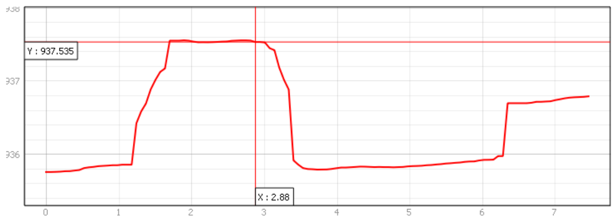

Figure 3.4.4-4: Top two rows: close ups on DEM generated by the four different processing software. The red lines indicate the location of the transect crossing car and snow wall. Third row: close-up on ortophoto generated by MOD_ODM software. Fourth row: elevation profile for a vertical cut of snow from a snow mower. Bottom row: profile of the center of the car on the left, same axis scale. Red for MOD_ODM, green for Sitescan, brown for Metashape, and blue for Datact.

3.5 Comparison using the Breiddalen#2 Phantom 4 dataset

To estimate the variability among drones and cameras, we compare results acquired with the DJI Matrice 300 with a DJI Phantom 4 RTK, using images acquired at the same location, within a reasonably short timeframe. The camera on the Phantom 4 has a rolling shutter redout delay (the fc6310r sensor), while the v2 DJI Zenmuse P1 sensor mounted on the M300 has a global shutter. This may (or may not) already be automatically adjusted for in the commercial processing software codes- depending on sensor type. This shutter redout delay can be measured[8]. The M300 camera sensor includes a full global shutter, which means that no delay should be necessary. For the MOD_ODM software, all data sets including the different UASs, were automatically created using the same initial settings.

3.5.1 Visual comparison

From the visual comparison, the RTK generated models have reference markers that are in the center for each ground control point, showing high horizontal accuracy. The centimeter margin of error is unknown. Calculated statistics from the SfM-models give a quantitative assessment of errors.

[8] https://github.com/horshack-dpreview/RollingShutter

Figure 3.5.1-1: Orthophoto with control points. Three points have been visually compared with the different datasets.

DJI M300 RTK

Point C

Point B

Point A (distance between red and black points: 8.1 cm)

DJI Phantom 4 RTK

Point C

Point B

Point D

Figure 3.5.1-2: Orthophoto with control points, showing georeferenced differences for the two independent datasets, left side, reference dataset#1 M300, right side, dataset#2 Phantom 4

3.5.2 Elevation transects using the Breidallen#2 Phantom 4 dataset

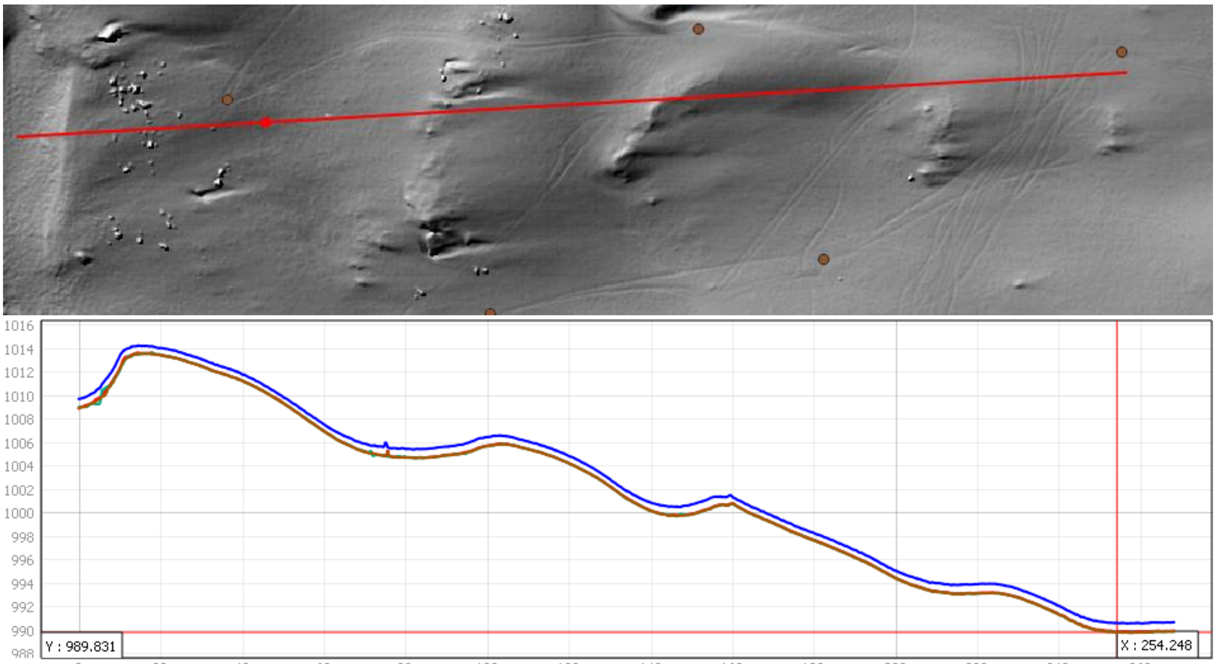

Figure 3.5.2-1: Transect of Phantom 4#1: slice and elevation profile for all four sets. Blue: Datact, Brown: Metashape, Turquoise: Sitescan, Red: MOD_ODM software.

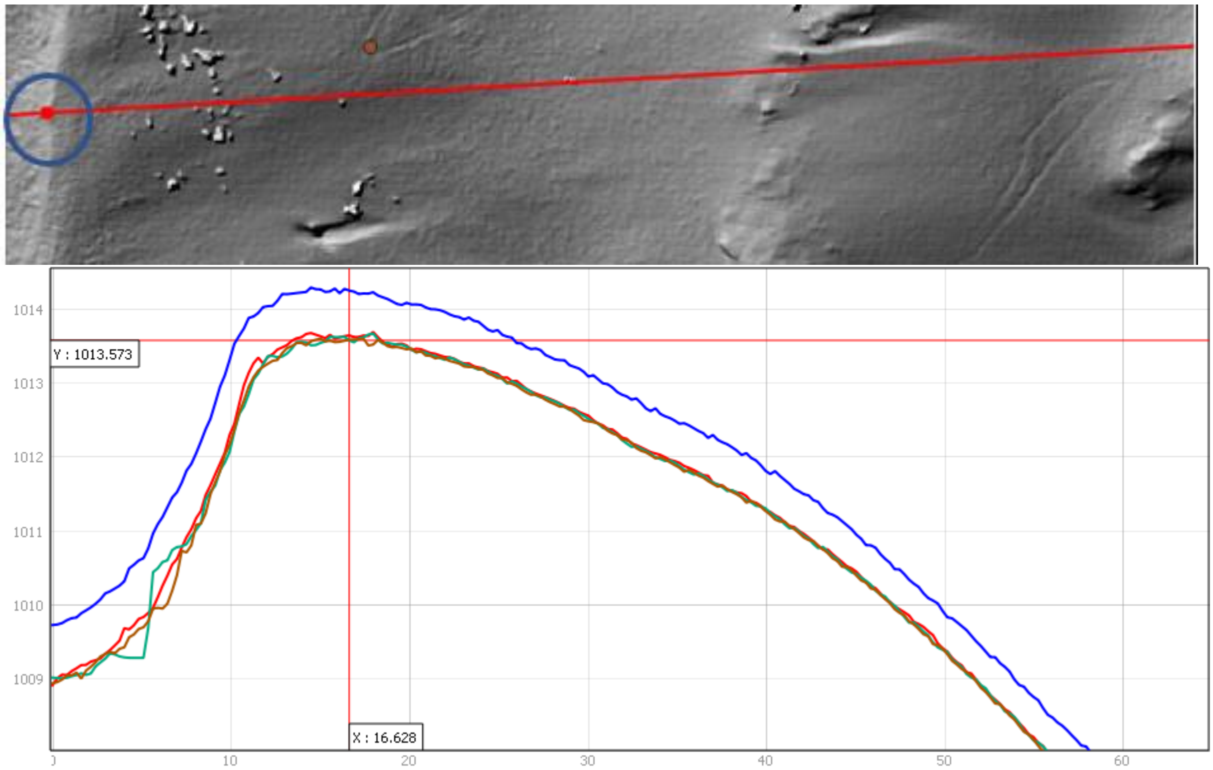

Figure 3.5.2-2: Transect of Phantom 4#1: slice and election profile for the four sets. Blue: Datact, Brown: Metashape, Turquoise: Sitescan, Red: MOD_ODM software.

The Datact shows a good general trend, but the curve is not smooth. The georeferencing error is also large, more than 60 cm difference from the other three runs. This data is not useful until the problem is resolved. The Sitescan has shown particularly reliable results previously. Here at the lower part of the "snowy hill" there are numerical artifacts which are caused by the lack of details in the raw images. This is easily fixed with the image enhancer algorithms.

From another section of the transect, the remaining three are close, Sitescan and MOD_ODM software only a few centimeters from each other, with some precision differences by Metashape processing. This does not mean that the Sitescan and MOD_ODM models necessarily are correctly aligned to the ground truth, as there may be systematic errors with the rolling shutter delay in the Phantom 4. At another part of the transect, the Sitescan (turquoise line) could not render the bush located as shown in Figure 3.5.2-3. This is again due to the problem with the raw images.

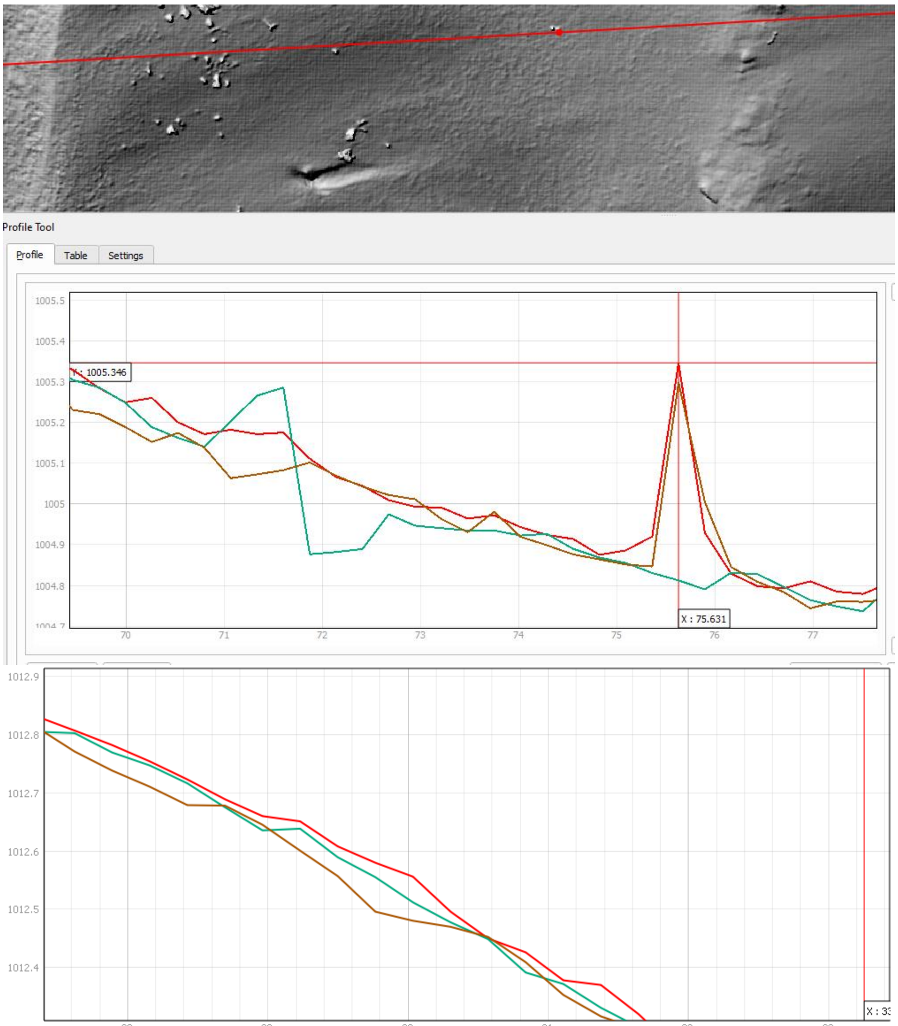

Figure 3.5.2-3: Top to bottom: DEM models showing an arbitrary transect, elevation profile of the transect and zoomed area

In Figure 3.5.2-4, another example is shown over a snowbank. Again, the rendering issues over white snow as seen with rendering problems for the Sitescan model. Interesting to see that Datact renders the surface well. Removing Datact and Sitescan, the Metashape and MOD_ODM models look the best, with deviations around +/- 5 centimeters.

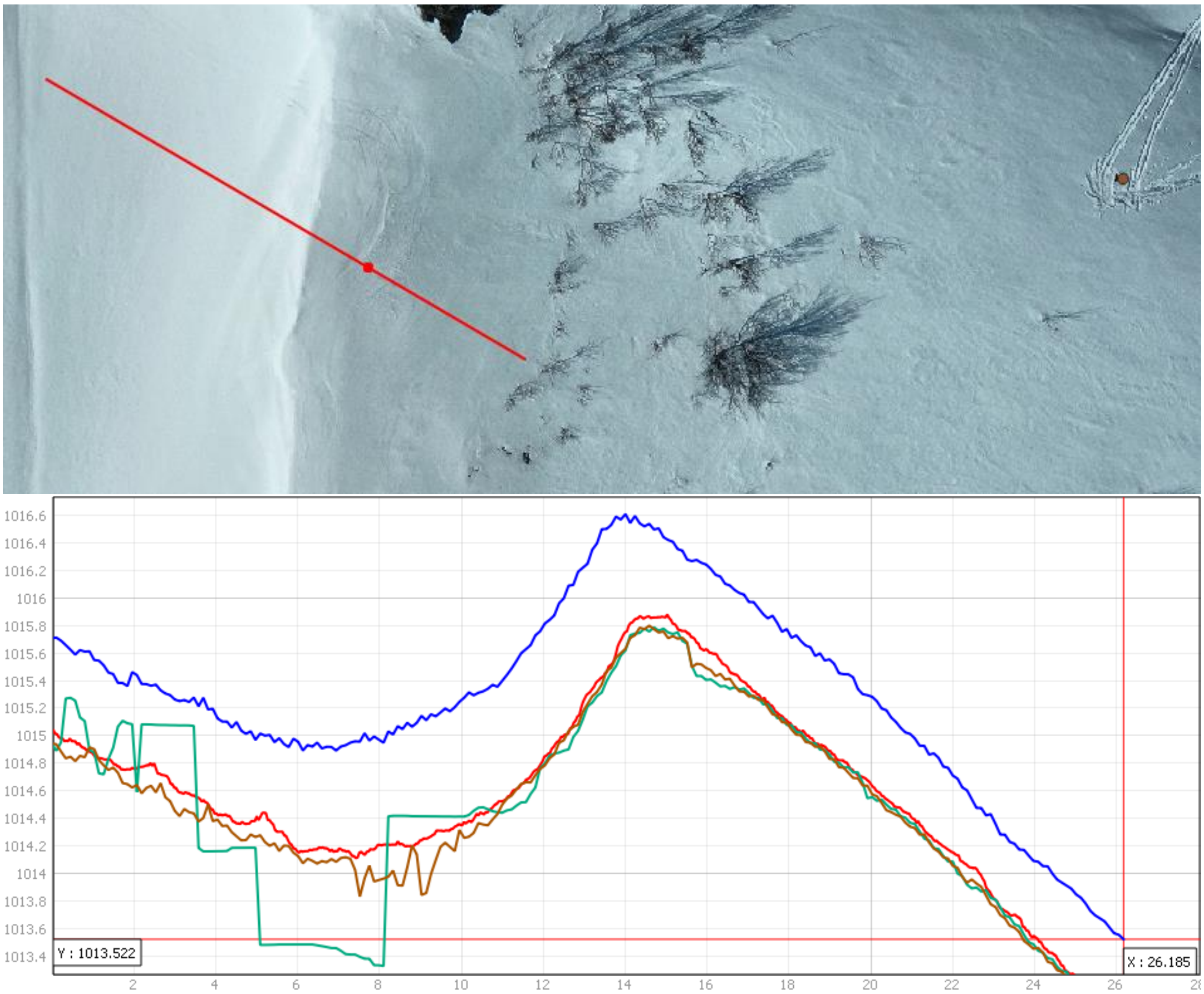

Figure 3.5.2-4: Transect along snow hill. Blue: Datact, Brown: Metashape, Turquoise: Sitescan, Red: MOD_ODM software.

3.6 Comparison of different UAS platform and camera payloads

In this section we compare the data acquired with the Matrice 300 UAS and Zenmuse P1 camera with the Phantom 4 UAS, using the same settings for processing.

3.6.1 Repeatability of surveys

A repeatability comparison was carried out with 6 datasets, 3 with the Phantom 4 UAS, and 3 with the M300. These runs were performed during a one-day period. The purpose here is to investigate repeatability, i.e., if the method is reliable at various times of the day and different light conditions. Note again that the pre-processing has been a necessary step to produce the following datasets.

The total deviation among all sets is on average -/+ 10cm (some of the runs have been run with lower resolution and different settings, not described here).

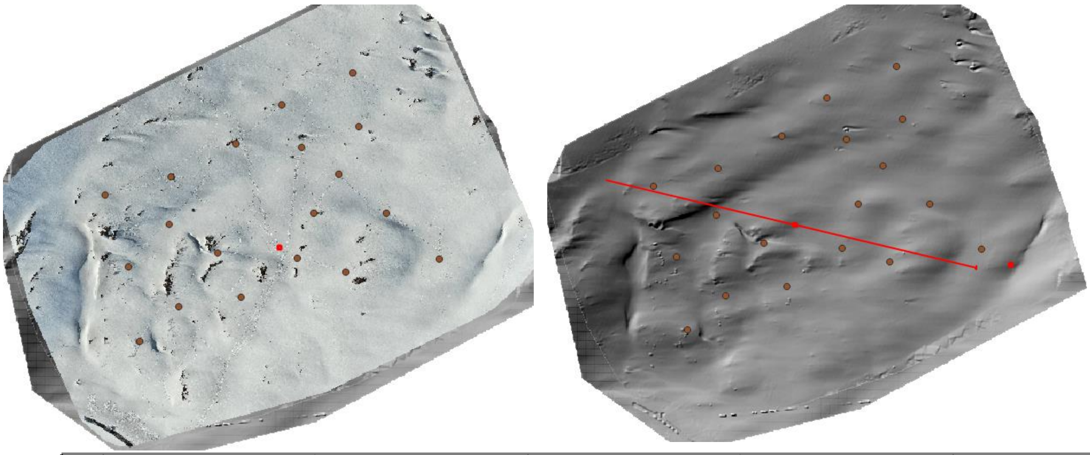

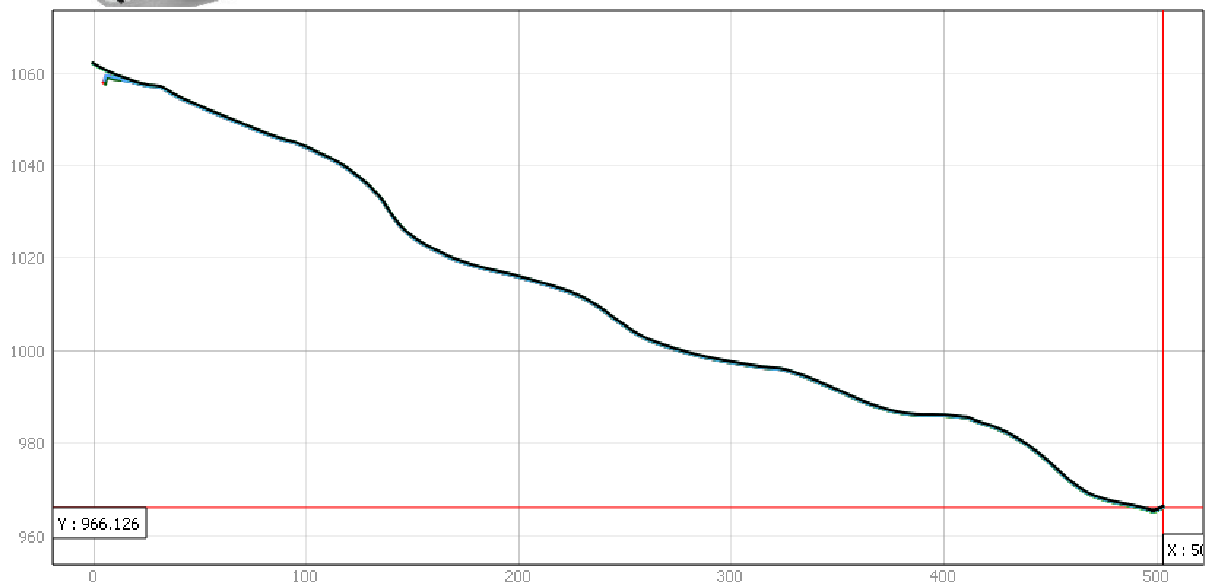

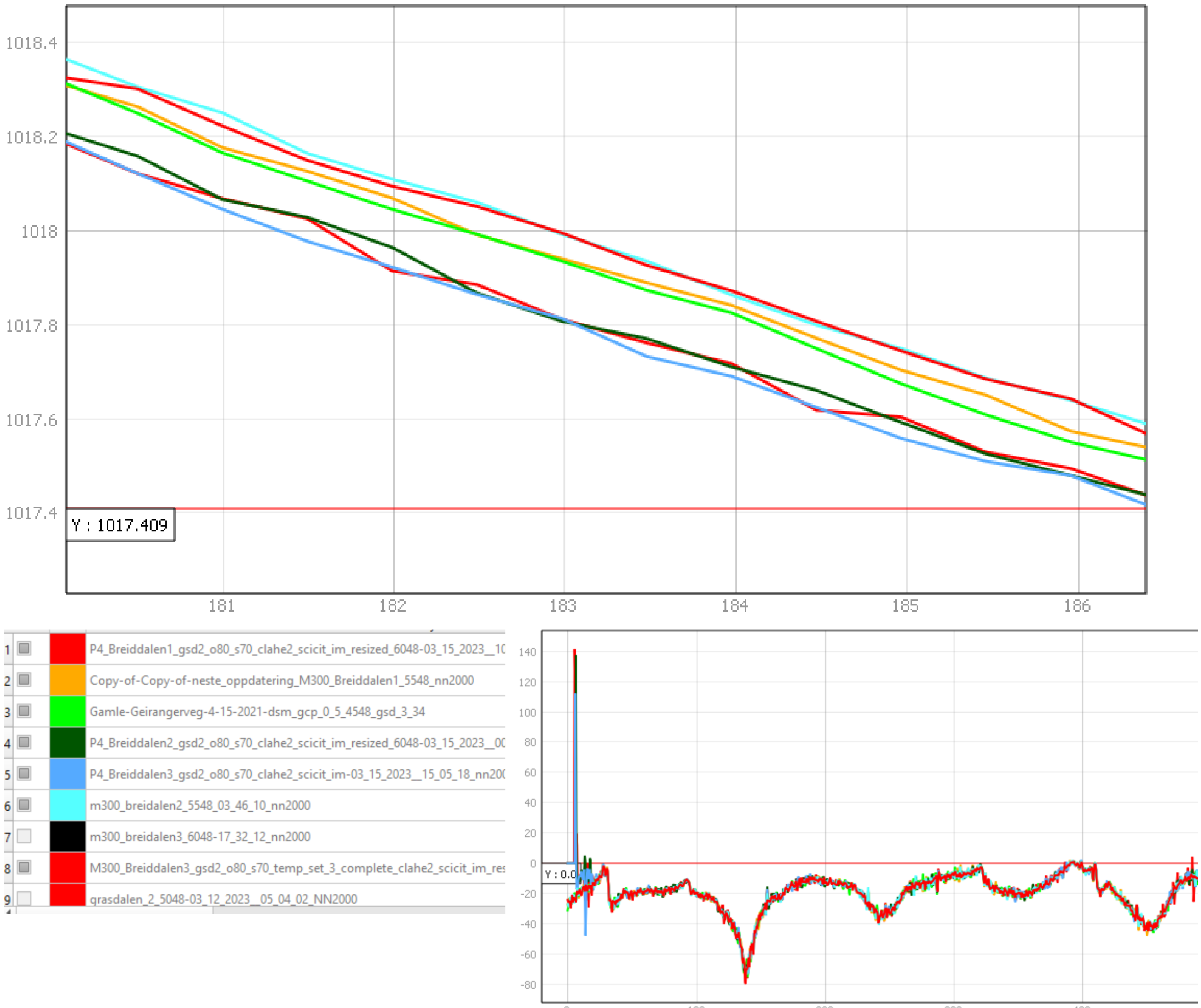

Figure 3.6.1-1: Comparison of M300 and Phantom 4 datasets taken over a period of one day, processed with the open-source method.

Appendix 1

Image projections for the study: All images are referenced as Tif raster with resolution 0,1 x 0,1 m in coordinate system ETRS89 / UTM zone 33, NN2000 (EPSG:5973)

Field test device

Below is described the pipeline used for creation of point cloud and DEM models that can be uploaded from the field using the uploader client.

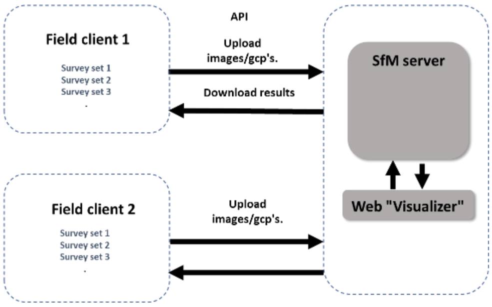

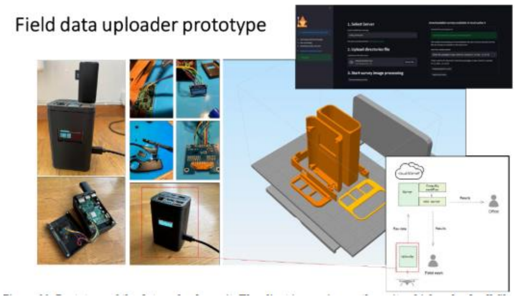

A prototype "field client" was tested consisting of a raspberry pi Linux board with a 4g-uploader. Images could be uploaded to the server for processing.

Preprocessing and Image Optimization for Snowy Terrain

Image Preprocessing after Acquisition

When acquiring images over snow using automated exposure settings (in auto or priority mode), the images often suffer from underexposure and white balance issues. These problems can lead to a loss of detail on snowy surfaces, which is critical for accurate tie-point matching in connected image pairs. While exposure compensation can address underexposure, both issues can be effectively corrected using histogram equalization techniques. UAS images, typically captured with auto-focus, are particularly prone to white balance problems.

To correct exposure issues—especially when dark areas are present amidst larger white snow patches—it is helpful to optimize the histogram for improved detail and highlight retention.

Initial photogrammetry tests, conducted without modifying the UAS imagery (from M300, Phantom 4 Pro, and Geodrones "Prototype One"), resulted in pixelated and noisy outputs. These issues introduced significant errors in the subsequent photogrammetry pipeline.

As a solution, pre-processing of the images was implemented in batch mode for the datasets. Several preprocessing methods were tested and scripted in Python. One particularly helpful method involved automatic brightness and contrast optimization followed by histogram clipping. This procedure included calculating the grayscale histogram, separating the RGB color channels, finding the cumulative pixel distribution, and finally clipping the histogram to generate a new image with an optimized histogram. Although this approach yielded significantly more detailed images, white balance issues persisted in areas with extensive white coverage. The method used for the surveys involved creating larger files with interpolated pixels, providing more detail and adaptability across the image. This method notably enhanced the visibility of tracks and details along snow layers.

The most effective technique for optimizing the images in the pipeline testes was Contrast Limited Adaptive Histogram Equalization (CLAHE), implemented using Python scikit-mage[9]. This adaptive histogram method significantly improved the detail in snow-covered surfaces. Unlike standard histogram equalization, Adaptive Histogram Equalization (AHE) computes several histograms corresponding to distinct sections of the image, redistributing lightness values to enhance local contrast and edge definitions. CLAHE, a variant of AHE, limits contrast amplification to mitigate noise.

The adaptive nature of CLAHE proved particularly efficient, treating different areas of the images uniquely and producing remarkable improvements in pixelation on some elevation models, especially over extensive snow-covered regions, compared to using the original non-optimized images. While integrating auto brightness correction with CLAHE could further enhance results, this was not explored in the current work.

To conclude, the implementation of adaptive histogram equalization techniques, specifically CLAHE, as part of the pre-processing pipeline, significantly improved the quality and detail of UAS imagery over snow-covered terrains. Future work could be explored combining this method with auto brightness adjustments for even better results.

Default image (Breidalen-3_DJI_20210415163708_0004)

[9] van der Walt, S., Schönberger, J. L., Nunez-Iglesias, J., Boulogne, F., Warner, J. D., Yager, N., Gouillart, E., & Yu, T. (2014). *scikit-image: Image processing in Python*. PeerJ, 2, e453. https://doi.org/10.7717/peerj.453

Final and best method used for the surveys. The method creates larger files, interpolates pixels with much more detail, but also adaptive along the image. Note that tracks are more visible and more details along the snow layers.

Figure 0-1: Contrast Limited Adaptive Histogram Equalization (CLAHE) implemented with skimage

Several methods were implemented and tested in the pre-processor, to run in batch for all images. The adaptive nature of this method means that the different areas of the images are treated differently. The difference in results on pixelation on the elevation models, especially over the larger areas of snow, were astonishing, compared to using the original non-optimized images. A further improvement is to mix the auto brightness code with CLAHE, this was not done in this work.

Statens vegvesen
Pb. 1010 Nordre Ål
2605 Lillehammer

Tlf: (+47) 22 07 30 00

firmapost@vegvesen.no

ISSN: 1893-1162